literature [see Refs. 4, 13, and 19(b)] to be of the order of T_2^{-k}. This indicates that the relevant time parameter is t'/T_2, i.e., that the decay of $K(t' \mid t_c)$ takes place on a time scale T_2. But regardless of these qualitative arguments, the rapid decay of $K(t' \mid t_c)$ is necessary in order that the decay of $G(t)$ be exponential, as observed experimentally.

[23]Both the infinite sum which defines the exponential operator and the infinite integral are associated with limiting processes, so the passage from Eq. (34) to Eq. (37) in the limit as $t_c/T_2 \to 0$ is by no means as obvious as it may at first appear. See Ref. 20 for a related discussion.

[24]J. M. Deutch and I. Oppenheim, in *Advances in Magnetic Resonance*, edited by J. S. Waugh (Academic, New York, 1968), Vol. 3, p. 43.

[25]One might wonder whether the inclusion of lattice motion in the theory would be capable of explaining a proportionality between $1/T^*$ and t_c. We have made some preliminary calculations of this type, and find that the inclusion of lattice motion does not appear to alter the situation materially. In particular, the leading term in a power-series expansion of $1/T^*$ is still proportional to t_c^4, just as in the present case [see Eq. (38)].

PHYSICAL REVIEW B VOLUME 6, NUMBER 9 1 NOVEMBER 1972

Proton Nuclear Magnetic Relaxation in Antiferromagnetic $NiCl_2 \cdot 6H_2O$, $CoCl_2 \cdot 6H_2O$, $CuCl_2 \cdot 2H_2O$, and $MnBr_2 \cdot 4H_2O$†*

I. J. Lowe and D. W. Whitson‡§
Department of Physics, University of Pittsburgh, Pittsburgh, Pennsylvania 15213
(Received 17 May 1972)

Proton-spin-lattice relaxation times (T_1) were measured by us in antiferromagnetic $NiCl_2 \cdot 6H_2O$ ($T_N = 5.34$ °K), $CoCl_2 \cdot 6H_2O$ ($T_N = 2.29$ °K), and $MnBr_2 \cdot 4H_2O$ ($T_N = 2.13$ °K) in the temperature range $4.18 - 1.12$ °K. Spin-echo experiments were also carried out over the same temperature range to determine the homogeneous transverse relaxation time T_2 in $NiCl_2 \cdot 6H_2O$ and the extent of the inhomogeneous broadening in $CoCl_2 \cdot 6H_2O$. Samples of various impurities and shapes were investigated. The spin-lattice relaxation time T_1 was found to be strongly temperature dependent for the first two crystals. The T_1 data from the $CoCl_2 \cdot 6H_2O$ crystals could be fit to a power law ($T_1 \propto T^{-7}$), but the T_1 data from the $NiCl_2 \cdot 6H_2O$ crystals could not. The temperature dependence of T_1 for $MnBr_2 \cdot 4H_2O$ was not determined because of the short temperature range over which we were able to make measurements. The temperature dependence of T_1 for the first two crystals along with the experimental results for $CuCl_2 \cdot 2H_2O$ ($T_N = 4.3$ °K) have been explained through a first-order two-magnon process plus a second-order three-magnon process. The second-order three-magnon process arises from the four-magnon exchange interaction which has been shown by Beeman and Pincus to completely supersede the first-order three-magnon process when $T > T_{AE}$. The impurity levels, the sample shape, and the orientation of an external magnetic field H_0 had no effect on the temperature dependence of T_1. In $NiCl_2 \cdot 6H_2O$ the value of T_2 measured from a 90°-90°-pulse-sequence experiment increased from a value of about 28 μsec at 4.18 °K to a value of about 65 μsec at 2.3 °K and then at 2.1 °K dropped to about 30 μsec and stayed at this value down to 1.12 °K. In $CoCl_2 \cdot 6H_2O$ the inhomogeneous broadening was dependent on the orientation of H_0 and the sample shape. An rf enhancement was found in $CoCl_2 \cdot 6H_2O$ for H_0 along the anisotropy axis (c axis).

I. INTRODUCTION

The first experimental measurements of the spin-lattice relaxation time T_1 for protons in antiferromagnetic materials were made by Hardeman *et al.*[1] Moriya[2] and Van Kranendonk and Bloom[3] tried to explain the dependence of T_1 on the absolute temperature T using a relaxation process due to the Raman scattering of magnons. Their results were of the right order of magnitude, but the temperature dependence was slower than the T^{-7} dependence found experimentally. Pincus and Winter[4] then proposed a theory which gave the T^{-7} temperature dependence but required $T \ll T_{AE}$, where $k_B T_{AE} = \hbar\omega_{AE}$ and $\hbar\omega_{AE}$ is the magnon energy gap. They assumed that the magnetostrictive terms in the Hamiltonian produced a magnon component in the thermal phonon spectrum allowing the phonons to participate directly in the relaxation processes. The T^{-7} temperature dependence in $CuCl_2 \cdot 2H_2O$ ($T_{AE} \simeq 1.4$ °K) covers the range $T > T_{AE}$ as well as the range $T < T_{AE}$. Other crystals, $CoCl_2 \cdot 6H_2O$ ($T_{AE} \simeq 2$ °K) and $KMnF_3$ ($T_{AE} \simeq 0.3$ °K), that have also exhibited this temperature dependence for T_1 have also included the range $T > T_{AE}$. In fact for $KMnF_3$ the middle of the temperature range is on the order of 100 times T_{AE}. Also, as is reported in Sec. IV, the temperature dependence of T_1 in $NiCl_2 \cdot 6H_2O$ cannot be fitted by a power law. Additional arguments and evidence against

using the magnon-phonon interaction to explain T_1 in the range $T > T_{AE}$ and, incidentally, for using it in the range $T < T_{AE}$ are given in Sec. V. The temperature dependence has been shown to be due to a combination of a first-order two-magnon process and a second-order three-magnon process. The second-order three-magnon process arises from the four-magnon exchange interaction which has been snown by Beeman and Pincus[5] to completely supersede the first-order three-magnon process when $T > T_{AE}$.

A T^{-7} dependence for T_1 was found by Abkowitz and Lowe[6] for the protons and by Cowen and Taylor[7] for the ^{35}Cl nuclei in $CoCl_2 \cdot 6H_2O$. For the F^{19} nuclei in $KMnF_3$ Mahler, Daniel, and Parrish[8] found a T^{-7} dependence for T_1 in a heavily doped sample (10 000 ppm) and a T^{-5} dependence for a lightly doped sample (30 ppm); along with a low-temperature exponential region in both samples. They suggested that the T^{-7} dependence was due to impurities and that the T^{-5} dependence and the low-temperature exponential region were intrinsic processes.

Because of these results in $KMnF_3$, we decided to check the effects of impurities on the temperature dependence of T_1 in $CoCl_2 \cdot 6H_2O$ and $NiCl_2 \cdot 6H_2O$. It was found that concentrations of 20, 400, and 30 000 ppm of paramagnetic impurities in $NiCl_2 \cdot 6H_2O$ had virtually no effect on the temperature dependence of T_1. Other ongoing experiments, which were continued, were the effects of the orientation of a constant external magnetic field H_0 on the temperature dependence of T_1 in $CoCl_2 \cdot 6H_2O$ and $NiCl_2 \cdot 6H_2O$. Also, the effects of sample shape were investigated in $CoCl_2 \cdot 6H_2O$. The results of these investigations were combined with the results for $CuCl_2 \cdot 6H_2O$, and a theoretical explanation of the three crystals was attempted.

While these investigations of T_1 were progressing the dependence of the inhomogeneous broadening on the orientation of H_0 and the sample shape was looked into for $CoCl_2 \cdot 6H_2O$. Also concurrently, the temperature dependence of the spin-echo transverse relaxation time T_2 was found in $NiCl_2 \cdot 6H_2O$.

In the following text it is to be understood that the crystals at all times, are in the antiferromagnetic region, i.e., $T < T_N$, where T_N is the Néel temperature. The Néel temperatures for $CuCl_2 \cdot 2H_2O$, $NiCl_2 \cdot 6H_2O$, and $CoCl_2 \cdot 6H_2O$ are 4.3, 5.34, and 2.29 °K, respectively.

II. EXPERIMENTAL TECHNIQUES AND PROCEDURES

A. Apparatus

The measurements reported in this article were taken with a coherent pulsed NMR spectrometer operating at 30.0 MHz. Details about the apparatus are described elsewhere.[9,10] A 90°-rf excitation pulse for protons was about 1 μsec long, and the apparatus recovery time following the pulse was about 3 μsec. The inhomogeneities of the applied static magnetic field H_0 were small enough [T_2 (magnet) $\approx$ 1 msec] that their effects on the measurements were negligible.

Conventional cryogenic techniques were used to cover a measuring temperature range of 1.12–4.18 °K. The samples were immersed in a liquid-helium bath contained in a glass Dewar pair. The bath was pumped on by a large mechanical pump through a large-aperture membrane-type regulator that could hold the helium vapor pressure above the bath to within several millidegrees of any desired temperature over the range covered. The helium vapor pressure was measured by two large-bore oil and mercury manometers that could be read to 0.1 mm. They were connected to a sensing probe that had a diameter large enough to eliminate the need for any thermomolecular corrections.

B. Measurement Techniques

The spin-lattice relaxation time T_1 was measured by applying a 90°-90°-pulse sequence and then observing the amplitude M of the free induction decay (FID) following the second pulse (a "90° pulse" nutates the spins by 90°). This amplitude M was measured as a function of the time t between the two pulses and obeys the law

$$M(t) = M(\infty)\,(1 - e^{-t/T_1})\ . \tag{1}$$

In some of the measurements (see Sec. IV A) a sequence of five 90° pulses was used to saturate the proton resonance line instead of one pulse. The time t in Eq. (1) would then be the time from the last of the saturating pulses to the measuring pulse.

For some measurements, the NMR lines were so inhomogeneously broadened that the FID following the 90° measuring pulse was too short to allow an accurate measurement of T_1 to be made. In these cases, a 90° pulse followed a time t later by a 90°-180°-pulse sequence separated by a time τ was used to generate an echo at time τ after the 180° pulse. The time sequence of events was thus: 90° pulse-t-90° pulse-τ-180° pulse-τ-echo. The peak height of the echo $M_E(t, \tau)$ is described by the equation

$$M_E(t, \tau) = M(t)\, e^{-2\tau/T_2}\ , \tag{2}$$

where T_2 is a spin-spin or transverse relaxation time. By holding time τ constant and varying time t, we may still determine T_1 by the dependence of the echo height on t using Eq. (1), with $M(\infty)$ being replaced by $M'(\infty) = M(\infty)e^{-2\tau/T_2}$.

The reported values for the spin-spin relaxation time T_2 were measured by observing the height of

the echo following the application of either a 90°-90°-pulse sequence or a 90°-180°-pulse sequence. The time between the second pulse and the echo peak was the same as the time t between the pulses. The amplitude of the echo $M_e(t)$ was measured as a function of t and obeyed the equation

$$M_e(t) = M_e(0)e^{-2t/T_2} . \quad (3)$$

C. Sample Preparation

Single crystals of $CoCl_2 \cdot 6H_2O$, $NiCl_2 \cdot 6H_2O$, and $MnBr_2 \cdot 4H_2O$ were grown at 40 °C from saturated aqueous solutions by the evaporation technique. The length of time to grow a $1\times1\times\frac{1}{2}$-cm crystal was about 2 weeks. The rate of success for $NiCl_2 \cdot 6H_2O$ and $CoCl_2 \cdot 6H_2O$ was about one "good" crystal a month, while the $MnBr_2 \cdot 4H_2O$ crystals were quite easy to grow. We considered a crystal "good" if it had four or more smooth faces and all the faces could be identified by measuring the angles between the faces. These angles are described in Groth.[11] The crystals had a marked tendency to twin, and some of the faces had a structure which resembled a brick wall in miniature. Most of the crystals were found to be of the same type as described by Groth. The faces of those crystals that had a different appearance were identifiable by measurement of the angles between the faces. The crystals were oriented through the identification of the faces. The magnetic field values necessary for resonance at 30 MHz in $CoCl_2 \cdot 6H_2O$ for different orientations of H_0 were measured and were found to agree very closely with the resonance diagrams given by Sawatzsky and Bloom.[12] We had no way to check the orientations of the $NiCl_2 \cdot 6H_2O$ and $MnBr_2 \cdot 4H_2O$ crystals, but such good success was had in orienting the $CoCl_2 \cdot 6H_2O$ crystals, that we feel reasonably certain that the orientations given in this article for these other crystals are correct to within ±5°.

The cylindrical samples were 7 mm diam and about 2 cm long. The "spherical" samples were 7 mm diam and not quite perfect spheres. However, we feel that they were good enough (that is different from cylinders) that any shape-dependent effects should have been observable. Details of the growing of these crystals and the production of the spherical samples are given in Ref. 13.

The high-purity samples were made from[14] cobalt "sponge" or high-purity Ni mixed with HCl and H_2O. The "impure" samples were reagent grade chemicals.[14] One $NiCl_2 \cdot 6H_2O$ crystal with 30 000 ppm of Co was made by mixing reagent grade $NiCl_2 \cdot 6H_2O$ and $CoCl_2 \cdot 6H_2O$. The $CoCl_2 \cdot 6H_2O$ samples for which measurements are reported were analyzed[15] by flame emission spectroscopy for impurities. The "pure" samples were found to contain 20 ppm of Fe, Cu, B. Si, and Ti. Traces of Al were also found. The "impure" samples of $CoCl_2 \cdot 6H_2O$ were found to have around 400 ppm of Fe and Ni. The crystals grown from reagent grade $NiCl_2 \cdot 6H_2O$ were not checked, but were assumed to have about the same impurity level as the $CoCl_2 \cdot 6H_2O$.

III. THEORY

A. Hamiltonian

For the purposes of computing the proton-spin-lattice relaxation time T_1 in these antiferromagnetic crystals, we shall use a two-sublattice model to describe the behavior of the electronic system and allow only nearest-neighbor exchange interactions. The starting Hamiltonian of the electron spin system is

$$\mathcal{H}_e = -2\sum_{l,m} J_{lm}(\vec{S}_l \cdot \vec{S}_m) - K(\sum_l S_{lz}^2 + \sum_m S_{mz}^2) - g\mu_B H_0(\sum_l S_{lz} + \sum_m S_{mz}) , \quad (4)$$

where the indices l and m are summed over the "up" and "down" sublattices, respectively. J_{lm} is the antiferromagnetic exchange integral, H_0 is the external applied magnetic field, K is the anisotropy constant, μ_B is the Bohr magneton, and g is the spectroscopic splitting factor.

The magnetic interaction between the electron system and the protons in these hydrated antiferromagnetic salts will be assumed to be dipolar. The Hamiltonian for the jth proton is

$$\mathcal{H}_N = -\hbar\gamma_N \vec{I} \cdot \{\vec{H}_0 - g\mu_B \textstyle\sum_l r_l^{-3}[\vec{S}_l - 3\vec{r}_l(\vec{r}_l \cdot \vec{S}_l)/r_l^2] - g\mu_B \textstyle\sum_m r_m^{-3}[\vec{S}_m - 3\vec{r}_m(\vec{r}_m \cdot \vec{S}_m)/r_m^2]\} , \quad (5)$$

where γ_N is the proton gyromagnetic ratio, $\vec{r}_l$ and $\vec{r}_m$ are the position vectors of the lth and mth electron spins relative to the position of the jth proton, r_l and r_m are their lengths, and $\vec{S}_l$ and $\vec{S}_m$ are the electron spins on the "up" sublattice and "down" sublattice, respectively. For convenience of notation the j subscript for the jth proton has been suppressed. Since the protons are part of a water molecule there is an additional proton-proton dipole interaction which in some cases is not negligible. However, neglect of this interaction, in what follows, does not lead to any serious consequences.

The electron spins will be broken up into two components as follows:

$$\vec{S}_l = \langle \vec{S}_l \rangle + \delta\vec{S}_l , \quad \vec{S}_m = \langle \vec{S}_m \rangle + \delta\vec{S}_m , \quad (6)$$

where $\langle \vec{S}_l \rangle$ and $\langle \vec{S}_m \rangle$ are the thermal averages of the lth and mth electron spins, respectively, and $\delta\vec{S}_l$ and $\delta\vec{S}_m$ are their fluctuating parts. The Hamiltonian then becomes

$$\mathcal{H}_N = \mathcal{H}_0 + \mathcal{H}' , \quad (7)$$

where

$$\mathcal{H}_0 = -\hbar\gamma_N \vec{I}\cdot\vec{H}_{eff}\ , \tag{8}$$

$$\vec{H}_{eff} = \vec{H}_0 - g\mu_B\textstyle\sum_l r_l^{-3}[\langle\vec{S}_l\rangle - 3\vec{r}_l(\vec{r}_l\cdot\langle\vec{S}_l\rangle)/r_l^2] - g\mu_B\sum_m r_m^{-3}[\langle\vec{S}_m\rangle - 3\vec{r}_m(\vec{r}_m\cdot\langle\vec{S}_m\rangle)/r_m^2]\ , \tag{9}$$

and

$$\mathcal{H}' = \hbar\gamma_N g\mu_B \vec{I}\cdot\{\textstyle\sum_l r_l^{-3}[\delta\vec{S}_l - 3\vec{r}_l(\vec{r}_l\cdot\delta\vec{S}_l)/r_l^2] + \sum_m r_m^{-3}[\delta\vec{S}_m - 3\vec{r}_m(\vec{r}_m\cdot\delta\vec{S}_m)/r_m^2]\}\ . \tag{10}$$

The diagonalization of the "static" part of $\mathcal{H}_N$, i.e., $-\hbar\gamma_N\vec{I}\cdot\vec{H}_{eff}$, will result in the spin energy-level splittings. The allowed transitions between these energy levels vary in frequency as a function of the angle between $\vec{H}_0$ and the crystal axes. The number of lines, i.e., transitions, for a given orientation of $\vec{H}_0$, depends on the number of inequivalent protons per unit cell. This behavior is exemplified by $CuCl_2\cdot 2H_2O$, with two water molecules per unit cell, and $CoCl_2\cdot 6H_2O$, with six water molecules per unit cell, as shown in Fig. 7 of Ref. 16 and Fig. 14 of Ref. 12, respectively. If the electronic g tensor is very anisotropic, as is the case in $CoCl_2\cdot 6H_2O$, then $\langle\vec{S}_l\rangle$ and $\langle\vec{S}_m\rangle$ are orientation dependent as well as field and temperature dependent.

B. Relaxation Mechanisms

The fluctuating part of the nuclear Hamiltonian $\mathcal{H}'$ causes transitions between the nuclear spin levels and provides the relaxation mechanism for protons to come to equilibrium with the lattice.

The two relaxation processes of interest here are Raman scattering, or two-magnon relaxation, and the exchange-enhanced three-magnon relaxation process. The one-magnon, or direct, relaxation process occurs when a magnon is absorbed or emitted as the nuclear spin is flipped. This process is usually forbidden in antiferromagnets due to energy considerations for the following reason. The magnon energy gap precludes the existence of any magnon with an energy less than $k_B T_{AE}$, and the smallest value of T_{AE} for the crystals under consideration is 1 °K. The equivalent temperature for a nuclear spin flip is, for a resonant frequency of $\omega_0/2\pi = 30$ MHz, $T_{nuc} = \hbar\omega_0/k_B \cong 10^{-6}$ °K. It is thus not possible to satisfy conservation of energy for a single-magnon process. More will be said about the possibility of the direct relaxation process in Sec. V.

In Raman-scattering processes, one spin wave is annihilated and another created while the nuclear spin jumps from one spin energy level to another. There is thus no problem of conserving energy, but a problem can arise with the conservation of the longitudinal component of spin angular momentum, since there is a nuclear spin flip with no net change in electron spin. The two-magnon process is forbidden[5] for nuclei of magnetic ions where the hyperfine interaction is isotropic and the axis of quantization of the nuclear spin and the electron spins are colinear. However, for the crystals under consideration, the Raman process is never forbidden since the nuclei interact with the electrons through dipole-dipole interaction.

In order for Raman scattering to occur, terms in the interaction Hamiltonian $\mathcal{H}'$ have to contain an I'^{+} or an I'^{-} (to flip the nuclei along $\vec{H}_{eff}$) multiplied by terms quadratic in the magnon operators, one of the operators an annihilator and the other a creator. The primed notation for I refers to the coordinate system whose z axis lies along $\vec{H}_{eff}$, as discussed in Appendix A.

The terms in $\mathcal{H}'$ which are of importance for two-magnon scattering involving a nuclear spin transition are then $I'^{+}\delta S_{lz}$, $I'^{-}\delta S_{lz}$, $I'^{+}\delta S_{mz}$, and $I'^{-}\delta S_{mz}$. The interaction Hamiltonian $\mathcal{H}_2'$ for the Raman process involving a nuclear spin transition is worked out in Appendix A and listed in Eq. (43). It contains the magnon creation and destruction operators a_l^+, a_l^-, b_l^+, and b_l^-. By transforming the boson operators into the ones which diagonalize the electron Hamiltonian and evaluating the matrix elements, Moriya[2] has found the thermal transition probability for a nuclear spin flip $-\frac{1}{2}\rightarrow\frac{1}{2}$, denoted by $W^{(2)}_{-1/2,1/2}$, due to Raman scattering, to be

$$W^{(2)}_{-1/2,1/2} = \tfrac{9}{16}\pi\left(\sum_l \frac{|h_l^+|^2}{r_l^6} + \sum_m \frac{|h_m^+|^2}{r_m^6}\right) \times \frac{h}{k_B}\,\frac{1}{\theta_m^6}\,(g\mu_B\gamma)^2 T^5 (4I_2)\ , \tag{11}$$

where θ_m is related to the maximum frequency by $\theta_m = \hbar\omega_m/(k_B T)$,

$$I_2 = \int_{x_{AE}}^{x_m}\left[\left(\frac{A_k}{k_B T}\right)^2 + x^2\right](x^2 - x_{AE}^2)\,\frac{e^x}{(e^x-1)^2}\,dx \tag{12}$$

and $x = (\hbar\omega)/(k_B T)$. The constant A_k is given by

$$A_k \simeq 2Sz|J|\ , \tag{13}$$

where z is the number of nearest neighbors. The limits of the integral I_2 are

$$x_{AE} = T_{AE}/T\ ,\quad x_m = \theta_m/T\ . \tag{14}$$

Identical calculations lead to the same form for $W^{(2)}_{1/2,-1/2}$ with $|h_l^+|^2$ and $|h_m^+|^2$ replaced by $|h_l^-|^2$ and $|h_m^-|^2$ so that $W^{(2)}_{1/2,-1/2} = W^{(2)}_{-1/2,1/2}$. Denoting the contribution to the proton-spin-lattice relaxation time due to Raman processes by $T_1^{(2)}$, we have

$$1/T_1^{(2)} = W^{(2)}_{1/2,-1/2} + W^{(2)}_{-1/2,1/2} = 2W^{(2)}_{-1/2,1/2}\ . \tag{15}$$

The three-magnon process occurs when one magnon is annihilated and two are created or two magnons are annihilated and one is created during a

nuclear spin transition. The standard three-magnon calculation carried out in Appendix A shows it to be about one order of magnitude less effective than the two-magnon process in producing nuclear relaxation. Since the two-magnon relaxation is never forbidden, in the crystals of interest here, the three-magnon process would not seem to be relevant to this discussion. However, Beeman and Pincus[5] have shown that this type of calculation severely underestimates the three-magnon process. There are, in fact, other mechanisms involving identical initial and final states in the scattering process which interfere constructively with the matrix elements calculated in Appendix A and thus enhance the three-magnon relaxation rate.

This enhancement process proceeds in two ways. (i) A virtual magnon is created from the direct relaxation process. This virtual spin wave of wave vector $\vec{k}_4$ then interacts with a thermal magnon of wave vector $\vec{k}_3$ via an exchange-scattering term, which is just the antiferromagnetic exchange interaction expanded to fourth order in magnons, and are scattered to new spin-wave states of wave vectors $\vec{k}_1$ and $\vec{k}_2$. (ii) Two thermal magnons of wave vectors $\vec{k}_1$ and $\vec{k}_2$ are scattered via the antiferromagnetic exchange-scattering term to one thermal magnon of wave vector $\vec{k}_3$ and a virtual magnon of wave vector $\vec{k}_4$. The virtual magnon is then absorbed as the nuclear spin flips via the direct relaxation process.

The effective interaction Hamiltonian is calculated by second-order perturbation theory by Beeman and Pincus[5] for the case of hyperfine interaction. Even though this process is second order, it completely supersedes the first-order three-magnon process calculated in Appendix A. The effect of the exchange enhancement is to supplement $I_3(T_{AE}/T)$ with $I_{ex}(T_{AE}/T)$. Both integrals are plotted in Fig. 4 in the paper by Beeman and Pincus. Equation (50) is now replaced by

$$W^{(3)}_{-1/2,1/2} = \frac{9\pi(27)}{8(2S)} \frac{(g\mu_B\gamma_N)^2}{\theta_m^6} \frac{\hbar}{k_B} \times\left(\sum_l \frac{|h_l^{\pm}|^2}{r_l^6}+\sum_m \frac{|h_m^{\pm}|^2}{r_m^6}\right)\left(\frac{A_k}{\theta_m k_B}\right)^3 T^5 \times\left[I_3\left(\frac{T_{AE}}{T}\right)+I_{ex}\left(\frac{T_{AE}}{T}\right)\right]. \quad (16)$$

It was also mentioned by Beeman and Pincus that Holstein has pointed out that repeated exchange scatterings may further enhance the relaxation rate. This additional effect would probably not be too important for antiferromagnetic ions of $S \gg 1$, but might affect the results for $S = \frac{1}{2}$ quite drastically, since each additional matrix element contributes a factor of $(2S)^{-1}$. Harris[17] has since considered the effect of these higher-order multiple spin-wave scatterings on T_1 in a ferromagnetic insulator. He carried the calculations to all orders in $1/S$ but to leading order in $k_BT/2JS$, K/J, μ_eH_0/J, etc. He found that the results of Beeman and Pincus are unaffected by the higher-order multiple scattering processes. This would seem to indicate that $W^{(3)}_{-1/2,1/2}$ would not be further enhanced until $T \to T_N$.

Beeman and Pincus have also calculated a dipolar-induced two-magnon process, which operates in the same way as the exchange-induced three-magnon process except that the initial and final states are the same as for a two-magnon process. This process, however, is considerably less effective than the regular Raman scattering in the crystals of interest here, so it will not be considered in what follows.

The two relaxation processes discussed here (two-magnon and exchange-enhanced three-magnon processes) seem to provide an adequate explanation of the experimental data reported in this paper.

C. Orthorhombic Symmetry and Other Considerations

The antiferromagnetic resonance data of two of the crystals considered ($CuCl_2 \cdot 2H_2O$[18,19] and $NiCl_2 \cdot 6H_2O$[20]) can be explained by arguments based on orthorhombic symmetry, while for the third, $CoCl_2 \cdot 6H_2O$,[21] one needed to assume in addition, a large anisotropic exchange interaction. This anisotropic behavior of $CoCl_2 \cdot 6H_2O$ is clearly shown in the respective g values of the three crystals: $g_a = 2.2$, $g_b = 2.23$, $g_c = 2.24$ for $CuCl_2 \cdot 2H_2O$,[22] $g_a \simeq g_b \simeq g_c = 2.2$ for $NiCl_2 \cdot 6H_2O$,[20] and $g_a = 2.9$, $g_b = 5.0$, $g_c = 4.0$ for $CoCl_2 \cdot 6H_2O$.[21] Even $CoCl_2 \cdot 6H_2O$ shows the same qualitative behavior as a crystal with orthorhombic symmetry. Therefore, it seems prudent to check if the orthorhombic symmetry has any affect on the thermal relaxation of protons in these crystals. This was done by us in detail for the two-magnon process in Ref. 13. The result was found to be

$$W^{(2)}_{-1/2,1/2} = \tfrac{9}{16}\pi\left(\sum_l \frac{|h_l^{\pm}|^2}{r_l^6}+\sum_m \frac{|h_m^{\pm}|^2}{r_m^6}\right)\frac{\hbar}{k_B}\frac{1}{\theta_m^6} \times(g\mu_B\gamma)^2 T^5(I_{2A}+I_{2B}+2I_{2C}), \quad (17)$$

where

$$I_{2A} = \int_{x_{AE_1}}^{x_m}\left[\left(\frac{A_k}{k_BT}\right)^2+x^2\right](x^2-x_{AE_1}^2)\frac{e^x}{(e^x-1)^2}\,dx,$$

$$I_{2B} = \int_{x_{AE_2}}^{x_m}\left[\left(\frac{A_k}{k_BT}\right)^2+x^2\right](x^2-x_{AE_2}^2)\frac{e^x}{(e^x-1)^2}\,dx, \quad (18)$$

$$I_{2C} = \int_{x_{AE_2}}^{x_m}\left[\left(\frac{A_k}{k_BT}\right)^2+x^2\right][(x^2-x_{AE_1}^2)(x^2-x_{AE_2}^2)]^{1/2}$$

$$\times \frac{e^x}{(e^x-1)^2}\,dx\ ,$$

and

$$x_{AE_{1,2}} = T_{AE_{1,2}}/T\ ,\quad x_m = \theta_m/T = \hbar\omega_m/k_BT\ .$$

If $T_{AE_1} = T_{AE_2} = T_{AE}$ then $I_{2A} = I_{2B} = I_{2C} = I_2$, and Eq. (17) reduces to Eq. (11). It will be shown in the discussion for $CuCl_2 \cdot 2H_2O$ that the inclusion of the orthorhombic symmetry in place of uniaxial symmetry makes very little difference in the results for $W^{(2)}_{-1/2,1/2}$. However if there were a great deal of difference between T_{AE_1} and T_{AE_2}, say a factor of 3 or greater, then inclusion of this symmetry could make a difference.

It should also be noted that the three-magnon exchange-enhanced process is more sensitive to the value of T_{AE}, and therefore, the inclusion of orthorhombic symmetry here could have an effect. This conjecture was not checked, because there are grosser approximations made for this relaxation process, e.g., the small-$\vec{k}$ approximation.

Since $\langle S_z \rangle$ is a strong function of temperature, especially for T near T_N, it would seem prudent to check the temperature dependence of $h_l^{\pm}$ defined by Eq. (41). This is done in Appendix B for $CuCl_2 \cdot 2H_2O$. As $T \to T_N$, it is found that the temperature dependence is negligible only because the small-$\vec{k}$ approximation introduces such a large error. This temperature dependence is notable only when $H_0 \sim |\vec{H}_d|$ ($|\vec{H}_d|$ is the dipole field of the electrons at the proton site) and is negligible for $H_0 \gg |\vec{H}_d|$ or $H_0 \ll |\vec{H}_d|$. $|\vec{H}_d|$ is of the order of 1 kG.

It was found necessary, especially for $NiCl_2 \cdot 6H_2O$, to consider the temperature dependence of T_{AE}. This is done in Appendix C.

In Appendix D the experimental T_1 data are fitted by the function

$$1/T_1 = C_1 e^{-\alpha_1/T} + C_2 e^{-\alpha_2/T}\ .$$

While it is possible to fit the data by this function for all three crystals, the values of α_1 are not consistent, and there is no theory to explain the origin of this function.

IV. EXPERIMENTAL RESULTS AND INTERPRETATION

A. $NiCl_2 \cdot 6H_2O$

1. Important Physical Parameters

The spin direction as determined by Kleinberg[23] with neutron diffraction and by Hamburger and Friedberg[24] with susceptibility studies was found to be 22.5° from the a' axis ($a' = b \times c$) towards the a axis. The magnetic ordering reported by Kleinberg is antiferromagnetic along the c axis and ferromagnetic along the a axis. The ion in the center of the $a-b$ plane is ordered antiferromagnetically with the corner ions. The lattice parameters are $a = 10.23$ Å, $b = 7.05$ Å, $c = 6.57$ Å, and $\beta = 122°10'$.

Since the crystals $NiCl_2 \cdot 6H_2O$ and $CoCl_2 \cdot 6H_2O$ are considered to be isostructural, the position of the protons will be assumed to be the same in both and the distances will be considered to be those found by Saffar[25] for $CoCl_2 \cdot 6H_2O$. The distance from the proton to the Ni (or Co) ion is assumed to be

$$r_l \simeq 2.7 \text{ Å} \tag{19}$$

and, thus,

$$\sum_l \frac{|h_l^{\pm}|^2}{r_l^6} + \sum_m \frac{|h_m^{\pm}|^2}{r_m^6} \simeq \frac{|h_1^{\pm}|^2}{r_1^6} \simeq 0.3 \times 10^{45}\ , \tag{20}$$

where the value of $|h_1^{\pm}|^2$ is taken from Eq. (66) in Appendix B.

From antiferromagnetic resonance[20] data, it is found that $H_E = 86$ kG. From this value

$$\frac{A_k}{k_B} \simeq \frac{2Sz_1|J|}{k_B} = \frac{g\mu_B H_E}{k_B} = 12.7\ ^\circ\text{K}\ , \tag{21}$$

where the g value is taken to be 2.2, $S = 1$, and $T_N = 5.34$ °K.

The value of $T_{AE}(0)$ that was used for calculating the two-magnon relaxation rate was 6.6 °K. This is an average of the two values $T_{AE} = 6.1$ °K and $T_{AE_2} = 7.1$ °K calculated from anisotropy fields $H_{A1} = 9.5$ kG and $H_{A2} = 12.5$ kG. The relationship used for this calculation was $T_{AE} = 2SZ_1|J| \times (2\alpha + \alpha^2)^{1/2}/k_B$, where $\alpha = H_A/H_E$. The reason for this choice of $T^{(2)}_{AE}$ (the superscript 2 stands for the two-magnon process) is that, as was mentioned in Sec. III C, the effect of orthorhombic symmetry in $CuCl_2 \cdot 2H_2O$ was negligible if the value of $T_{AE}(0)$ was chosen to be the mean value of T_{AE_1} and T_{AE_2}.

The value of $T_{AE}(0)$ chosen for the three-magnon process was 6.1 °K. The value 1.26 °K was subtracted from $T^{(3)}_{AE}$ at each temperature. The 1.26 °K represents the depression of the spin-wave energy gap due to the applied field, i.e., $H_0 \cong 8.5$ kG, and this depresses the energy gap by about $g\mu_B H_0$. This was not done for the two-magnon value because as the gap for one spin-wave branch is depressed another is raised. In calculating the integral I_2 this would average out just as it did when orthorhombic symmetry was considered. The integral $I_{ex}(T_{AE}/T)$ is, however, much more strongly dependent on the value of T_{AE}, and it is felt that the lowest-energy gap might dominate. It was found necessary to either choose this value of $T^{(3)}_{AE}$ or else to choose a lower value of θ_m in order to fit the data. The choice of θ_m affects the value of $1/T_1^{(3)}$ because

$$\frac{1/T_1^{(3)}}{1/T_1^{(2)}} = \frac{27}{S}\left(\frac{A_k}{\theta_m k_B}\right)^3 \frac{I_3}{4I_2}\ ,$$

and the relative importance of $1/T_1^{(3)}$ goes up for smaller values of θ_m. Also $1/T_1^{(2)} \propto 1/\theta_m^6$ so that if a smaller value of θ_m was chosen the final value of $1/T_1^{(2)}$ would have had to have been reduced by some factor (greater than 1) in order to fit the data. Another alternative would have been to multiply $1/T_1^{(3)}$ by some arbitrary factor in order to increase it as was done for the $CuCl_2 \cdot 2H_2O$ data. This last alternative may not be too unreasonable because Eq. (52) was simply an order-of-magnitude estimate. It is not clear at this point which of the above three methods, if any, is the most reasonable, but it is the first one mentioned above which is used here. The θ_m found from fitting the experimental points for $1/T_1^{(2)}$ is $\theta_m = 13.0\ ^\circ\mathrm{K}$. Thus to sum up:

$$T_{AE}^{(2)} = 6.6\ ^\circ\mathrm{K}, \quad T_{AE}^{(3)} = 6.1\ ^\circ\mathrm{K},$$

and (22)

$$\theta_m = 13.0\ ^\circ\mathrm{K}.$$

The temperature dependence of T_{AE} will be assumed to be that in Fig. 7 (Appendix C). This is a reasonable approximation because the temperature dependence of $\langle S_z \rangle$ is the same for all three crystals,[26] i.e., $\langle S_z \rangle_0 - \langle S_z \rangle \propto T^4$.

2. *Comparison of $1/T_1$ Data with Theory*

The relaxation rate is given by

$$1/T_1^{(2,3)} = 2W_{-1/2,1/2}^{(2,3)},$$

where $W_{-1/2,1/2}^{(2,3)}$ are given by Eqs. (11) and (16). Using the parameters listed in Sec. IV A 1 we find

$$1/T_1^{(2)} = 1.28 \times 10^{-3} T^5 I_2$$

and (23)

$$1/T_1^{(3)} = 1.26 \times 10^{-2} T^5 [I_{ex}(T_{AE}/T) + I_3(T_{AE}/T)].$$

The $1/T_1$ found from adding $1/T_1^{(2)}$ and $1/T_1^{(3)}$ in Eq. (24) is lower than the experimental values by a factor of 2.4. Thus each of these values is multipled by 2.4, and the theoretical lines plotted in Fig. 1 are

$$1/T_1^{(2)} = 3.07 \times 10^{-3} T^5 I_2,$$

(24)

$$1/T_1^{(3)} = 3.02 \times 10^{-2} T^5 [I_{ex}(T_{AE}/T) + I_3(T_{AE}/T)].$$

This is not an unreasonable thing to do since Hardeman *et al.*[1] have shown that T_1 changes by a factor of 5 in $CuCl_2 \cdot 2H_2O$ just due to change in the orientation of $\vec{H}_0$. Also $|h_1^{\pm}|^2$ was estimated for $CuCl_2 \cdot 2H_2O$, and the difference between the environment of a proton in $CuCl_2 \cdot 2H_2O$ and $NiCl_2 \cdot 6H_2O$ could easily account for a factor of 2.4.

The overshoot of $1/T_1^{(3)}$ as $T \to T_N$ can be laid at the doorstep of the small-$\vec{k}$ approximation. Beeman and Pincus[5] made two calculations of the first-order three-magnon process relaxation rate of F^{19} in MnF_2, one using the exact spin-wave density of states and the other using the small-$\vec{k}$ approximation. Figure 5 in their paper shows that the small-$\vec{k}$ approximation overshoots the exact calculation in much the same way as the calculated $1/T_1^{(3)}$ rate overshoots the experimental data in Fig. 1.

The result of taking T_{AE} as a function of temperature instead of as a constant is illustrated in Table I. When it is realized that $I_{ex}(T_{AE}/T)$ is a more sensitive function of T_{AE} than is I_2, the necessity of considering the temperature dependence of T_{AE} becomes clear, and thus, this was done in plotting the theoretical curves in Figs. 1, 3, and 4.

The temperature dependence of $|h_1^{\pm}|^2$ in the calculations for Table I is negligible since $H_0 \cong 8.5$ kG $\gg |\vec{H}_d|$. It has been reported[26] that $T_{AE} = 4\ ^\circ\mathrm{K}$ fits the specific-heat data very well. If $T_{AE} = 4\ ^\circ\mathrm{K}$ was used here, the $1/T_1^{(2)}$ relaxation points would not have the right temperature dependence (too slow) but the $1/T_1^{(3)}$ relaxation would give values of about the right size. More will be said about this in Sec. V.

The effect of impurities was found to be negligible. Three samples were studied: (i) 30-ppm impurity, (ii) 400-ppm impurity, and (iii) 30 000-ppm impurity. The impurities were paramagnetic ions and are discussed in Sec. II C. There was found to be no discernible difference between the relaxation times of the first two samples, and only a slight difference between these and the third as seen in Fig. 1. This difference will be more fully discussed in Sec. V.

Two different orientations were investigated: (a) $H_0 \| z$ (where z is the easy axis) and (b) H_0 about 65° from the z axis. These orientations are correct to within about 10°. The temperature dependence of the relaxation times remained the same,

TABLE I. T_{AE}, $I_2[T_{AE}(T)]$, and $I_2(T_{AE} = 6\ ^\circ\mathrm{K})$ as a function of T for $NiCl_2 \cdot 6H_2O$.

T (°K)	1.0	1.2	1.5	2.0	2.5	3.0	3.5	4.0
$T_{AE} = f(T)$	6.0	6.0	6.0	5.9	5.75	5.53	5.13	4.68
$I_2[T_{AE} = f(T)]$	22.6	36.7	52.6	63.2	59.9	52.3	45.9	39.9
$I_2[T_{AE} = 6.0\ ^\circ\mathrm{K}]$	22.6	36.7	52.6	60.7	54.9	45.2	35.8	28.1

but the value of $1/T_1$ for $H_0 \| z$ axis was 1.5 times larger than for the other orientation. This is quite easily explained by a shift in the value of $|h_1^+|^2$ when the orientation was changed. The data in Fig. 1 are those taken with $\vec{H}_0$ about 65° from the z axis.

Since the lines in $NiCl_2 \cdot 6H_2O$ are so close together that they create beats on the FID, it was decided to use a multiple-pulse sequence to measure T_1. Instead of using a single 90° pulse to saturate the proton NMR line, a series of five pulses was used. Measurements were also taken with the regular two-pulse sequence. Some differences did occur between the two methods for the temperature range 2.6 to 3.6 °K. The two processes ($1/T_1^{(2)}$ and $1/T_1^{(3)}$) cross each other in this temperature range. The experimental results of the two-pulse sequence followed the theoretical predictions more closely in this region than did the multiple-pulse sequence. The two-pulse and multiple-pulse data points were the same throughout the rest of the temperature range. This difference is probably due to some form of cross relaxation. In $CoCl_2 \cdot 6H_2O$ the effect of the multiple-pulse method was checked for a line far enough from all other lines so that there was no interference problems. The results were no different than for the single-pulse method. There is a slight but not dramatic difference between the heavily doped (30 000 ppm) sample from the other two.

It should be mentioned here that the T_1 data from $NiCl_2 \cdot 6H_2O$ do not fit any power-law dependence.

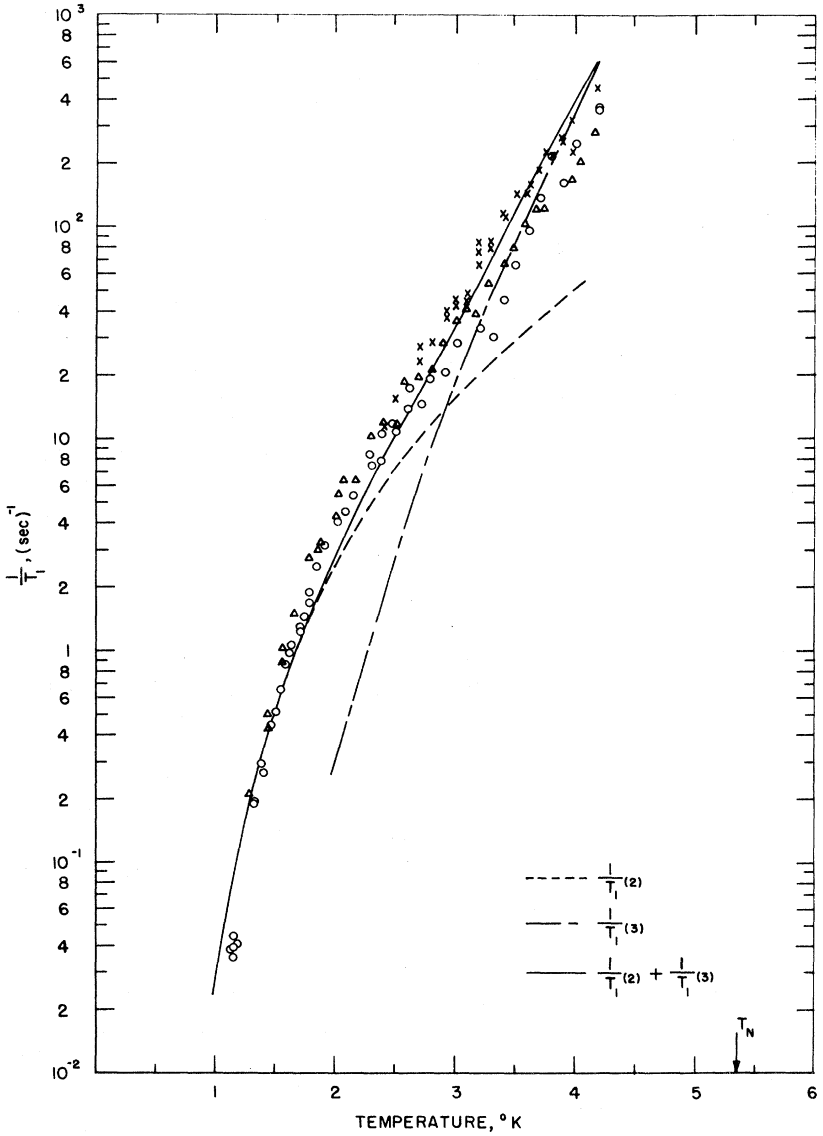

FIG. 1. $\text{Log}_{10}(1/T_1)$ vs T for $NiCl_2 \cdot 6H_2O$. The circles and the ×'s are the experimental points found when five pulses and one pulse, respectively, were used to saturate the line in the pure sample (20 ppm). The triangles are the data from the 30 000-ppm sample using five pulses.

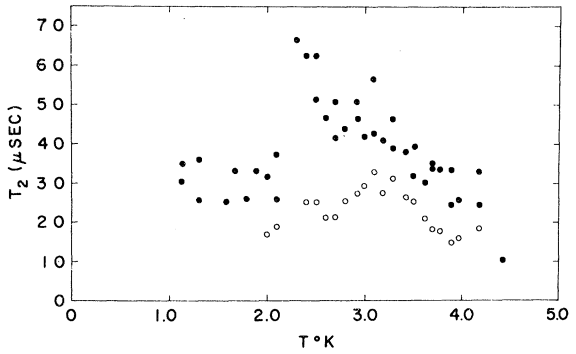

FIG. 2. Spin-spin relaxation time T_2 as a function of temperature for $NiCl_2 \cdot 6H_2O$. The open and closed circles are 90°–180° and 90°–90° echoes, respectively.

3. *Spin-Spin Relaxation Times*

The spin-spin (or transverse) relaxation time T_2 as found from the spin-echo experiment is plotted against temperature in Fig. 2. From 4.18 to 2.3 °K the value of T_2 from the 90°-90°-pulse sequence increases from a value of about 28 to a value of about 65 μsec. Below 2.3 °K, it drops rapidly, so that by 2.1 °K, the value of T_2 is 30 μsec, and it stays at this value down to 1.12 °K. The 90°-180°-pulse sequence gives values of T_2 almost a factor of 2 smaller than the values found from the 90°-90°-pulse sequence. If a drop in the 90°-180° T_2 occurs below 2.3 °K it is not as dramatic as the drop in the 90°-90° T_2 and is obscured in the scatter of the data.

The temperature dependence of T_2 in $CoCl_2 \cdot 6H_2O$ has been reported by Abkowitz and Lowe.[7] It does not show any sharp dropoff of T_2 in the temperature range investigated.

B. $CoCl_2 \cdot 6H_2O$

1. *Important Physical Parameters*

The magnetic ordering for $CoCl_2 \cdot 6H_2O$ is the same[23] as in $NiCl_2 \cdot 6H_2O$ except that the spin direction is now the c axis and $a = 10.34$ Å, $b = 7.06$ Å, $c = 6.67$ Å.

The proton distances for $NiCl_2 \cdot 6H_2O$ is assumed to be the same as for $CoCl_2 \cdot 6H_2O$, and thus the value of $|h_1^{\pm}|^2/r_1^6$ is that computed in Eq. (20).

An average value for the exchange integral is assumed as

$$A_k/k_B = 2S|J_1|z_1/k_B \cong 5\ ^\circ\mathrm{K}\ .$$

It is found[27] that the exchange integral is quite anisotropic and has the above value for H_0 along the a' axis ($a' = b \times c$). The proton relaxation data in Fig. 3 was taken with H_0 nearly along the a' axis.

From antiferromagnetic resonance[21] data T_{AE1} can be found to be 1.66 °K (using the value of 34.63 GHz as the lower energy gap with $H_0 = 0$). Since the resonance parameters are so complicated for $CoCl_2 \cdot 6H_2O$ it was difficult to decide what to use for T_{AE2}. Taking the values for $NiCl_2 \cdot 6H_2O$ and $CuCl_2 \cdot 2H_2O$ as a guide, we set $T_{AE}^{(2)} = 2.0$ °K and $T_{AE}^{(3)} = 1.66$ °K. The orientation of $\vec{H}_0$ was perpendicular to the easy axis (c axis), and therefore, the depression of the magnon energy gap was ignored. Also, the resonance diagrams are so complicated compared to $NiCl_2 \cdot 6H_2O$ and $CuCl_2 \cdot 2H_2O$ that it is hard to tell what effect the application of an external field has on the magnon energy gap. The temperature dependence of T_{AE} will be taken from Fig. 7.

The value of θ_m used ($\theta_m = 5.0$ °K) was chosen to be consistent with that used for $NiCl_2 \cdot 6H_2O$. Moriya[2] gives a formula for θ_m:

$$\theta_m = \{[(A_k/k_B)\eta(3\pi^2)^{1/3}]^2 + T_{AE}^2\}^{1/2}\ . \qquad (25)$$

Using the values given for $NiCl_2 \cdot 6H_2O$ in Sec. IV A it was found that $\eta \cong 0.3$. This value of η gives $\theta_m \cong 5.0$ °K for $CoCl_2 \cdot 6H_2O$. Since η is a geometric factor and $CoCl_2 \cdot 6H_2O$ and $NiCl_2 \cdot 6H_2O$ are isomorphic, θ_m will be taken as 6.0 °K.

Since $\vec{H}_0$ was along the a' axis the g value was taken $g \cong g_{a'} = 2.7$ (g is also quite anisotropic[28]). For $CoCl_2 \cdot 6H_2O$ the effective spin is $\frac{1}{2}$, and $T_N = 2.29$ °K.

2. *Comparison of $1/T_1$ Data with Theory*

In Fig. 3 the proton relaxation data from this lab have been supplemented by the ^{35}Cl-spin-lattice relaxation data of Cowen and Taylor.[7] (The raw data were kindly supplied by Cowen and Taylor.) The $1/T_1$ ^{35}Cl data have been multiplied by 1.42 so that they overlap the proton data in the temperature range where data points from both experiments exist.

The gyromagnetic ratio of the ^{35}Cl nucleus is about 0.1 that of the proton, however the magnetic coupling between the electrons and the ^{35}Cl nucleus is transferred hyperfine (which is usually a factor of 10 larger than dipole-dipole coupling). The size of the transferred hyperfine field can be estimated from the resonance frequency of Cowen and Taylor's experiment ($f = 7.6$ MHz at 1.15 °K) since only a small (20 G) external magnetic field was applied. The transferred hyperfine field is about 18 kG. This means that the magnitude of the $1/T_1$ data for ^{35}Cl should be $(1.8)^2 = 3.2$ times larger than the magnitude of $1/T_1$ data for the protons (the dipole-dipole field is about 1000 G). Hardeman *et al.*[1] have shown that $1/T_1$ increases by as much as a factor of 5 in $CuCl_2 \cdot 2H_2O$ when H_0 is increased. The proton data for $CoCl_2 \cdot 6H_2O$ were taken with $H_0 \sim 8.5$ kG. Also, for hyperfine[5] and transferred hyperfine interaction $1/T_1 \propto \sin^2\theta$, where θ is the angle between the axis of quantiza-

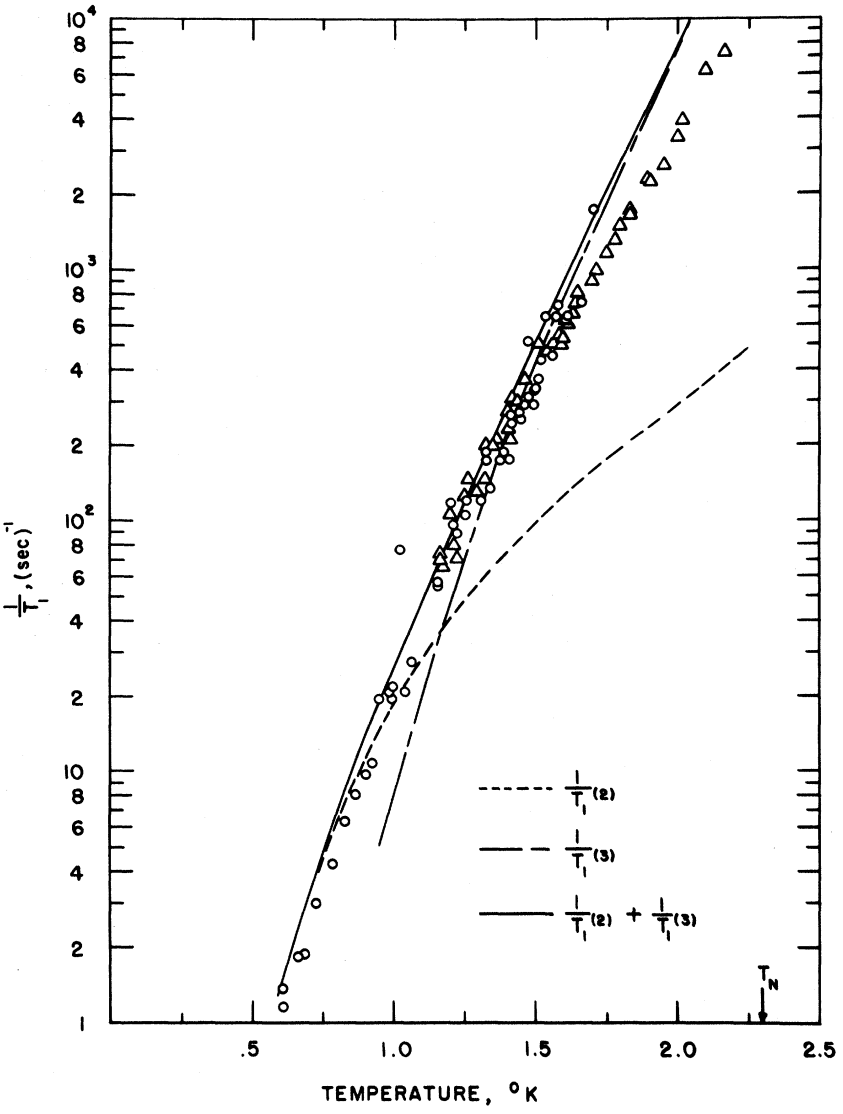

FIG. 3. $\text{Log}_{10}(1/T_1)$ vs T for $CoCl_2 \cdot 6H_2O$. The triangles and the circles are the data points for the proton and the ^{35}Cl resonance, respectively.

tion of the nuclei and the z axis (axis of quantization for the electron spins). This has been shown by Kaplan *et al.* to hold very well in MnF_2.[29] These two effects could easily account for the magnitude of the data for ^{35}Cl.

With the parameters from Sec. IV B 1 the relaxation times are

$$1/T_1^{(2)} = 0.93\ T^5 I_2 \tag{26}$$

and

$$1/T_1^{(3)} = 12.6 T^5 [I_{ex}(T_{AE}/T) + I_3(T_{AE}/T)] . \tag{27}$$

In order for $1/T_1$ to match the data at $T = 0.6$ and 3.3 °K the values of $1/T_1^{(2)}$ had to be divided by 1.5 and the values of $1/T_1^{(3)}$ had to be divided by 3.3. The values as plotted in Fig. 3 are

$$1/T_1^{(2)} = 0.62 T^5 I_2$$

and

$$1/T_1^{(3)} = 3.9 T^5 [I_{ex}(T_{AE}/T) + I_3(T_{AE}/T)] . \tag{28}$$

The fit is again very good, with the small-$\vec{k}$ approximation again causing an overshoot as $T \to T_N$.

Four different crystals of $CoCl_2 \cdot 6H_2O$ were intensively investigated: two "pure" samples (20 ppm), one a cylinder and the other a sphere, and two "impure" samples (400 ppm), again one a cylinder and the other a sphere. The impurities are given in Sec. II C.

There was found to be no differences at all in the temperature dependence of $1/T_1$ for these crystals. Only when the orientation of the crystal relative to the magnetic field was changed, was there any effect, and then, just as for $NiCl_2 \cdot 6H_2O$, only the magnitude of the relaxation changed, but not the temperature dependence. These changes in

TABLE II. List of $1/T_1$ results at 1.2 °K for four different crystals of $CoCl_2 \cdot 6H_2O$. Angle ϕ is the orientation of H_0 with respect to a' axis ($a' = b \times c$). The symbol ϕ_{min} after some orientations means that the particular line being measured is at the angle ϕ having the minimum frequency value given in Figs. 14 and 15 of Ref. 12. Ratio column is the value of $1/T_1$ normalized to the $1/T_1$ value for line 1, $\phi = \phi_{min} = 173°$ for the impure cylinder (data points plotted in Fig. 3).

Sample	Plane	Line No.	ϕ	$1/T_1$(sec)$^{-1}$	Ratio
"Impure"	a-c	1	173° (ϕ_{min})	88	1.0
cylinder		1	159°	85	0.96
(400 ppm)		2	173°	52	0.59
		2	206° (ϕ_{min})	59	0.67
		3	173°	19	0.22
		4	173°	16	0.18
		7	173°	36	0.41
		8	173°	77	0.88
		···	$H_0 \parallel c$ axis ($H_0 > H_c$)	460	5.26
"Impure"	a-c	1	173° (ϕ_{min})	87	0.99
sphere		2	200°	38	0.43
(400 ppm)		8	173°	79	0.90
		···	$H_0 \parallel c$ axis ($H_0 > H_c$)	480	5.45
		···	$H_0 \parallel c$ axis ($H_0 < H_c$)	85	0.97
"Pure"	a'-b	1	221° (ϕ_{min})	122	1.39
cylinder		(1, 2, 7, 8)	95°	190	2.16
(20 ppm)		2	181°	55	0.63
		4	95°	105	1.19
Pure	?	1	?	190	2.16
sphere		8	?	94	1.07
(20 ppm)					

magnitude for different orientations are given in Table II. Due to experimental difficulties the orientation of the "pure" sphere was unknown. For $\vec{H}_0 \parallel c$ axis, the magnitude of H_0 was about 8500 G for $H_0 > H_c$ and 6200 G for $H_0 < H_c$.

For each of the orientations and crystals listed in Table II, $1/T_1$ was found as a function of temperature between $1.14 < T < 2.2$ °K. The temperature dependence was, in each and every case, the same as plotted in Fig. 3.

One of the most striking changes in value occurs for $H_0 \parallel c$ axis for $H_0 < H_c$ and $H_0 > H_c$. This jump is due to the "spin-flop" phenomenon. For $H_0 < H_c$ the electron spins are aligned along the c axis, but for $H_0 > H_c$ the spins flop over perpendicular to the c axis. This change in direction of the electron spins causes the change in magnitude of the relaxation times.

In Fig. 14 of Ref. 12, lines number 3 and 4 are due to protons farther away from the Co ions than the protons represented by lines number 1, 2, 7, and 8. Therefore, as expected, their values of $1/T_1$ are less than for line number 1.

It is obvious from Table II that the shape of the crystal has very little or nothing to do with the magnitude of $1/T_1$. Combined with the knowledge that the temperature dependence of $1/T_1$ is the same for all these lines, one can safely say that the shape of the crystal is not important in $1/T_1$ measurements.

In trying to calculate the change in magnitude of $1/T_1$ for different orientations of $CoCl_2 \cdot 6H_2O$, it must be remembered that not only does $|h_1^+|^2$ change but that g is also highly anisotropic.

3. *Linewidth as a Function of Orientation*

Spin-echo experiments and analysis of the FID were undertaken in order to determine the linewidth as a function of orientation. It was found that the "homogeneous" transverse relaxation time T_2 (as determined from 90°-90° and 90°-180° pulse sequences) was not a function of orientation or of sample shape. For both the "impure" sphere and cylinder samples, the value of T_2 was 20 ± 5 μsec for line number 1 at $T \simeq 1.70$ °K for all orientations. Both the 90°-90° and 90°-180° pulse sequences gave the same value for T_2. This just indicates that the homogeneous linewidth does not depend on sample shape or orientation. The inhomogeneous broadening does, however, depend on the sample shape and orientation. This dependence is shown in Table III. The FID is exponential and T_2' is the characteristic decay time. The maximum value for T_2' occurs only for $|\phi_{min} - \phi| \leq 2°$ and decreases as $|\phi_{min} - \phi|$ is increased.

The component of the dipole field perpendicular to $\vec{H}_0$, $|\vec{H}_d|_\perp$, is a minimum at $\phi = \phi_{min}$ and increases as $\phi_{min} - \phi$ increases, reaching a maximum where the line crosses the "free" proton resonance. All this is highly suggestive of an inhomogeneous demagnetizing field set up by $|\vec{H}_d|_\perp$ which becomes more homogeneous as the shape of the crystal tends toward a perfect sphere or an ellipsoid. (Our "spherical" sample was not perfectly spherical, but was closer to that shape than was the cylinder.)

The difference in T_2' between the sphere and the cylinder for $\phi = \phi_{min}$ is probably due to $\vec{H}_d$ not being fully in the a-c plane. For if $\vec{H}_0$ was parallel to $\vec{H}_d$, T_2' should be the same for the two shapes and should be around 15 or 20 μsec.

It should be mentioned that this behavior is qualitatively the same for all the lines that were investigated (including those in $NiCl_2 \cdot 6H_2O$).

TABLE III. Free-induction-decay time T_2' for $CoCl_2 \cdot 6H_2O$ at $T \simeq 1.70$ °K (ϕ and ϕ_{min} are defined in Table II).

Sample	Orientation (ϕ)	T_2' (μsec)
"Impure"	173° (ϕ_{min})	8
sphere	150°	3.3
	123°	1.8
"Impure"	173° (ϕ_{min})	5.2
cylinder	163°	2.8
	153°	1.9

4. Enhancement of the rf Signal for $H_0 \| c$ Axis

For $H_0 \| c$ axis in $CoCl_2 \cdot 6H_2O$ the rf signal is enhanced, i.e., the 90° pulse for $H_0 \| c$ axis is shorter than the 90° pulse for other orientations. The 90° pulse is defined as the pulse duration necessary to nutate the nuclear magnetization 90 deg. The rf enhancement for $H_0 < H_c$ ($H_0 \cong 6000$ G) is about 1.2 and for $H_0 > H_c$($H_0 \cong 8500$ G) is about 1.6, i.e., for $H_0 > H_c$ the 90° pulse was about 1.0 μsec long while the regular 90° pulse is about 1.6 μsec.

This sort of rf enhancement has been seen elsewhere[28,30] for $H_0 > H_c$. It has been explained through the rocking of the electron magnetization by the rf excitation field. When H_0 is rotated by a small angle θ in the spin-flop state ($H_0 > H_c$) the sublattice magnetizations M_1 and M_2 remain perpendicular to the applied field and rotate through the angle θ. If an rf magnetic field H_{rf} is applied in the plane defined by $\vec{M}_1$, $\vec{M}_2$ and $\vec{H}_0$, and perpendicular to $\vec{H}_0$, the total applied field $\vec{H}_T$ is rotated through an angle $\theta = H_{rf}/H_0$. The total field $\vec{H}_T$ is then rocked at the radio frequency. This causes a similar rocking of $\vec{M}_1$, $\vec{M}_2$ and consequently the interaction field (dipole or hyperfine) H_N experienced by the nuclei, through the same angle θ at the radio frequency. Thus, for the hyperfine case the nuclei are driven indirectly by an additional rf field of magnitude

$$h_{rf} = \theta H_N = (H_N/H_0)H_{rf} \ . \tag{29}$$

For the hyperfine case, this additional rf field is perpendicular to the original rf field and about 100 times as large. Thus, the additional rf field is the one which determines the resonance, and the original rf field is negligible. Also, since H_N is about 100 times H_0, it is H_N which essentially determines the axis of quantization for the nuclear spin.

The situation for the protons in the hydrated antiferromagnets under consideration is quite different. The magnetic field which determines the axis of quantization is

$$\vec{H}_{eff} = \vec{H}_0 + \vec{H}_d \ , \tag{30}$$

where $\vec{H}_d$ is the dipole field seen by the protons due to the electrons. When $H_0 > H_c$ the spins flop over perpendicular to $\vec{H}_0$, and there would again be a rocking effect. The effect on the proton spins is complicated by the dipole coupling but an estimate of the rf enhancement can be made by assuming that the direction of change of $\vec{H}_d$ is the same as the direction of the original rf signal. Thus, assuming $H_d = H_N \cong 1$ kG and $H_0 = 8.5$ kG, we have

$$1 + H_N/H_0 \cong 1 + \tfrac{1}{8.5} \cong 1.12 \ . \tag{31}$$

This is not large enough to explain the enhancement factor for $H_0 > H_c$, but it may be that the dipole coupling somehow enhances this effect more than the hyperfine coupling would.

For the case of $H_0 < H_c$, as H_0 approached H_c it might be expected that $\vec{M}_1$ and $\vec{M}_2$ would be rocked by a change in the total applied field, leading to an enhancement factor as found. This conjecture is strengthened by the results in $NiCl_2 \cdot 6H_2O$ where no rf signal enhancement was found. The critical field for $NiCl_2 \cdot 6H_2O$ is about 40 kG while H_0 was only 8.5 kG. From these numbers, it seems likely that for $CoCl_2 \cdot 6H_2O$ no enhancement effect would be discernible for low enough H_0.

5. Spin-Locking Effect

A spin-locking effect for the F^{19} nuclear resonance in antiferromagnetic $KMnF_3$ has been reported by Mahler and James.[31] In an external magnetic field they found that not only is a spin-echo signal observed for two short (3-μsec) rf pulses, but when the second pulse is increased (3–2000 μsec) there is also a spin-echo signal which always appears the same time after the completion of the second rf pulse. The nuclear relaxation time ($T_{1\prime}$) during the "locked" period was measured by them to be $T_2 \ll T_{1\prime} \ll T_1$, where $T_2 = 34$ μsec, $T_1 = 70$ msec, and $T_{1\prime} = 1.5$ msec.

We checked this effect for the F^{19} resonance in CaF_2 and the proton resonance in paramagnetic and antiferromagnetic $CoCl_2 \cdot 6H_2O$. For CaF_2 the external magnetic field was deliberately made quite inhomogeneous by introducing a 1-in. steel bolt into the air gap. The results for these two crystals were qualitatively the same as those found by Mahler and James. The T_2's found in CaF_2 and $CoCl_2 \cdot 6H_2O$ (~30 μsec) did not change when the second pulse was lengthened as long as the time t in Eq. (3) was the distance between pulses.

These results can be explained through a simple spin-locking effect, i.e., the spins do not lose phase coherence during the time the second pulse is applied, and is not limited only to antiferromagnetic crystals.

C. $CuCl_2 \cdot 2H_2O$

1. Important Physical Parameters

The symmetry of $CuCl_2 \cdot 2H_2O$ has been determined by Harker[32] by x-ray analysis to be orthorhombic with lattice parameters: $a = 7.38$ Å, $b = 8.04$ Å, and $c = 3.72$ Å. Neutron diffraction studies by Shirane *et al.*[33] have shown that the Cu^{++} ions are antiferromagnetically coupled along the c axis, in a sort of a chain, and that they are coupled ferromagnetically in the a-b plane.

The proton positions[34] have also been found from neutron-diffraction experiments, and the distance from a Cu^{++} ion to the nearest proton is $r_1 = 2.58$ Å, giving $|h_1^+|^2/r_1^6 = 0.4 \times 10^{45}$.

Hewson *et al.*[35] found $|J_1|/k_B = 6.78\,^\circ\mathrm{K}$ through a Green's-function method using the parameters $T_N = 4.33\,^\circ\mathrm{K}$ and $\theta = -5\,^\circ\mathrm{K}$, where θ is the Curie–Weiss constant.

The value of $T_{AE}^{(2)}(0)$ is set equal to $1.4\,^\circ\mathrm{K}$ which is the average of $T_{AE_1}(0)$ and $T_{AE_2}(0)$ found in Appendix C and $T_{AE}^{(3)}(0) = T_{AE}^{(1)}(0) = 0.975\,^\circ\mathrm{K}$. The temperature dependence of T_{AE} is also found in Appendix C.

The value of g is isotropic and is taken to be 2.2. The value of θ_m found by fitting the two-magnon relaxation rate to the low-temperature data is $20\,^\circ\mathrm{K}$, which happens to agree with Moriya's estimate[2] of $\eta = 0.5$.

2. *Comparison of Experimental Data and Theory*

The proton-spin-lattice relaxation times for $CuCl_2 \cdot 2H_2O$ in Fig. 4 were taken from Hardeman *et al.*[1] Using the parameters given in Sec. IV C 1 and

$$A_k/k_B \cong 2Sz_1|J_1|/k_B \cong 2|J_1|/k_B \cong 2(6.78) \qquad (32)$$

yields

$$1/T_1^{(2)} = 2.04\times 10^{-4}\, T^5 I_2\,. \qquad (33)$$

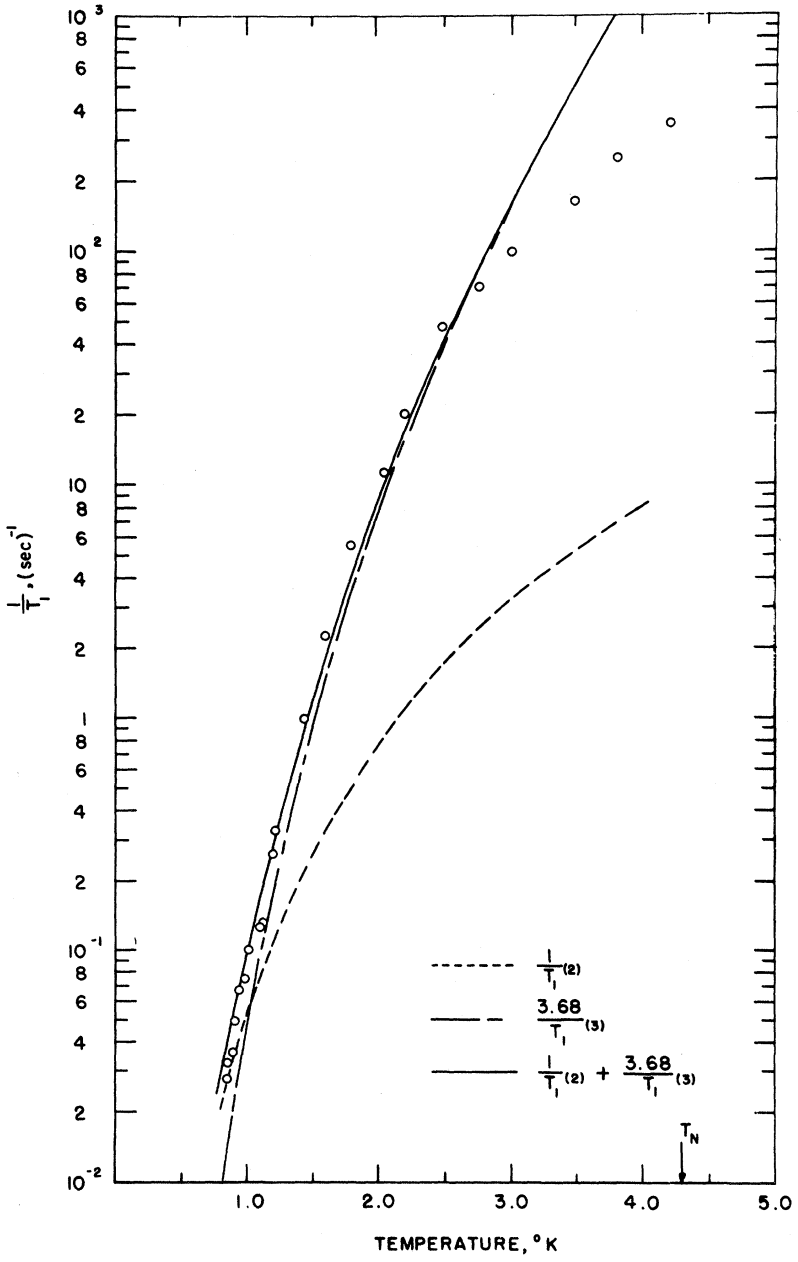

FIG. 4. $\mathrm{Log}_{10}(1/T_1)$ vs T for protons in $CuCl_2 \cdot 2H_2O$. The data are taken from Hardeman *et al.* (Ref. 1).

TABLE IV. I_2, $I_3(T_{AE}/T)$, and $I_{ex}(T_{AE}/T)$ vs T for $CuCl_2 \cdot 2H_2O$.

T(°K)	0.8	1.0	1.2	1.5	2.0	2.5	3.0	3.5	4.0
I_2	311	261	218	171	122	92	72	57	46
$I_3(T_{AE}/T)$	2.3	2.6	3.6	4.5	5.9	6.3	6.4	6.5	6.6
$I_{ex}(T_{AE}/T)$	6.6	13.2	20.0	35.0	74.0	128	204	300	520

The exchange-enhanced three-magnon relaxation rate is

$$1/T_1^{(3)} = 8.46\times 10^{-4}\, T^5 [I_{ex}(T_{AE}/T) + I_3(T_{AE}/T)] . \quad (34)$$

In order to obtain a better fit to the experimental data, the three-magnon rate has arbitrarily been given an additional enhancement factor of 3.68, and $3.68/T_1^{(3)}$ is the rate that has been plotted in Fig. 4. Almost exactly the same fit is obtained if we take $\theta_m = 19\,^\circ$K, $T_{AE}^{(2)} = 1.4\,^\circ$K, $T_{AE}^{(3)}(0) = 0.98\,^\circ$K, and the depression of the magnon energy gap due to H_0 = 1705 G (equivalent to 0.25 °K) is subtracted from $T_{AE}^{(3)}$ for each temperature. In this case $1/T_1^{(3)}$ only has to be multiplied by 2. An even better fit is obtained with the above choices for $T_{AE}^{(2)}$ and $T_{AE}^{(3)}$ but with $\theta_m = 15\,^\circ$K. In this case $1/T_1^{(3)}$ does not have to be multiplied (or divided) by anything, but the computed values of $1/T_1$ have to be divided by 6.2 to fit the experimental data. Since $|h_1^+|^2$ was calculated using the parameters for $CuCl_2 \cdot 2H_2O$, there does not seem to be any good reason for doing this. Therefore the last fit mentioned was not seriously considered. For $\theta_m = 19\,^\circ$K we have η = 0.45 and for $\theta_m = 15\,^\circ$K, $\eta = 0.36$. The latter value is closer to the values for $CoCl_2 \cdot 6H_2O$ and $NiCl_2 \cdot 6H_2O$ but the other two values (for $\theta_m = 19$ and 20 °K) are closer to Moriya's rough estimate.

For the case of $CuCl_2 \cdot 2H_2O$, additional enhancement might be expected, as discussed in Sec. III B, because $S = \frac{1}{2}$ for the Cu^{++} ion. However, if Harris[17] is correct there is no help from repeated exchange scatterings. His expansion is to leading order in $k_B T/2JS$, and the extra enhancement is needed down to about 1 °K. Since $T_N = 4.3\,^\circ$K, the higher-order terms in his expansion would not help much. This additional enhancement could of course be due to the approximation made in Eq. (52). There is an overshoot of the calculated values above the experimental values here just as for the other two crystals. Some typical values of I_2, $I_3(T_{AE}/T)$, and $I_{ex}(T_{AE}/T)$ are listed in Table IV. The values of I_3 and I_{ex} were taken from Fig. 4 in Beeman and Pincus.[5]

3. *Effect of Orthorhombic Symmetry*

The effect of using orthorhombic symmetry instead of uniaxial symmetry in the two-magnon process is shown in Table V. The value of $T_{AE}(0)$ used for calculating I_2 was 1.4 °K. For this process the difference is completely negligible. However since $I_{ex}(T_{AE}/T)$ is much more sensitive to the value of T_{AE}, as seen in Fig. 4 of Beeman and Pincus,[5] the orthorhombic symmetry might play a role. This type of calculation would, however, probably only give corrections to second order, compared to other corrections such as using the correct dispersion relation in place of the small-$\vec{k}$ approximation. For this reason no attempt was made to deduce the effect of orthorhombic symmetry on the three-magnon process.

D. $MnBr_2 \cdot 4H_2O$

Even though the Néel temperature of $MnBr_2 \cdot 4H_2O$ is 2.13 °K, we were not able to see a signal until 1.57 °K, a temperature gap of 0.56 °K. By contrast, there is a gap of only 0.09 °K in $CoCl_2 \cdot 6H_2O$ ($T_N = 2.29\,^\circ$K). Apparently, the dipole-dipole coupling is not as strong in $MnBr_2 \cdot 4H_2O$ as it is in $CoCl_2 \cdot 6H_2O$. What little experimental data we took are listed in Table VI.

V. SUMMARY AND DISCUSSION

The theoretical fit to the experimental data for each of the three crystals was reasonable. In each case the theory produced an overshoot of the experimental data as $T \to T_N$. This is believed to be due to the small-$\vec{k}$ approximation.

It was seen that the temperature dependence of T_{AE} cannot be neglected, and that the temperature dependence of $|h_1^+|^2$ (the orientation dependent part of the magnetic coupling) is of second order only when compared to the small-$\vec{k}$ approximation.

TABLE V. $4I_2$ and $(I_{2A} + I_{2B} + 2I_{2C})$ vs T for $CuCl_2 \cdot 2H_2O$.

T(°K)	0.8	1.0	1.2	1.5	2.0	2.5	3.0	3.5	4.0
$4I_2$	1.24×10^3	1.04×10^3	872	680	476	347	260	198	156
$I_{2A}+I_{2B}+2I_{2C}$	1.24×10^3	1.04×10^3	869	681	476	347	260	197	157

TABLE VI. T_1 vs T for $MnBr_2 \cdot 4H_2O$.

T(°K)	1.57	1.53	1.42	1.37	1.37	1.16
T_1(μsec)	18.2	14.7	15.0	26.3	55.3	36.0

Even if the correct dispersion relation were used, the temperature dependence of $|h_1^+|^2$ would, however, only be notable when $H_0 \sim H_d$ and as $T \to T_N$.

On the other hand, it was found that the type of crystal anisotropy used, orthorhombic or uniaxial, made very little difference in the two-magnon relaxation rate.

The values of $I_{ex}(T_{AE}/T)$, the integral for the exchange-enhanced three-magnon relaxation process, were taken from Fig. 4 in Ref. 5. Harris[36] has also calculated the exchange-scattering enhancement of the three-magnon process. His expansion of the spin waves is to lowest order in $1/z$ (where z is the number of nearest neighbors) instead of to lowest order in $1/2S$. He finds that the enhancement factor is about 8 for both $T \ll T_{AE}$ and $T \gg T_{AE}$ and not the strongly temperature-dependent integral $I_{ex}(T_{AE}/T)$. He claimed that some errors made by Beeman and Pincus[5] caused the discrepancy.

The theoretical fit reported in this text must remain in doubt until the above mentioned discrepancy is obviated and a more realistic dispersion relation is used in the calculation in place of the small-$\vec{k}$ approximation.

However, this fit is more attractive than the T^{-7} dependence or the equation, $1/T_1 = C_1 e^{-\alpha_1/T} + C_2 \times e^{-\alpha_2/T}$, reported in Appendix D. The most damaging experimental evidence against the T^{-7} fit is that the $NiCl_2 \cdot 6H_2O$ data cannot be explained with a power-law dependence. At the present time there is no theory to explain the fit of the double exponential. Also, the size of α_1 required by the three crystals is not consistent with their values of T_{AE} (see Appendix D).

One of the attractive aspects of the theory presented in the main body of text is that all the physical parameters used for the calculation, with the exception of θ_m, were those found from other experiments. Even though the parameter θ_m was chosen in order to get the best fit to the experimental data, all of the values of θ_m so found were quite reasonable.

As was mentioned in Sec. I, the T^{-7} temperature dependence was found in the range $T > T_{AE}$ for the crystals discussed, while the theory predicting a T^{-7} dependence[4] is only applicable to the range $T \ll T_{AE}$. Kimura[37] has carried out a detailed calculation of the specific heat of an antiferromagnet in the temperature range $T < T_{AE}$. He considered magnon-phonon interactions and showed that if one assumed a strong interaction, the specific-heat data[26] of $CoCl_2 \cdot 6H_2O$ in the temperature range $T < T_{AE}$ could be explained. Kimura[37] found that one of the allowed modes goes to zero as $\vec{k}$ goes to zero. This mode is the one that prevents the (specific heat)/T^3 of an antiferromagnet from going to zero as $T \to 0$ as predicted by Eisele and Keffer.[38] This mode would also allow the direct relaxation process to occur which heretofore had been forbidden by the conservation of energy and the magnon energy gap. This direct relaxation process, according to Pincus and Winter,[4] would give $T_1 \propto T^{-1}$. Benoit and Renard[39] have, in fact, found just such a temperature dependence for $CuCl_2 \cdot 2H_2O$ in the temperature range $T < 0.9$ °K ($T_{AE} \cong 1.5$ °K).

The T_1 data for $NiCl_2 \cdot 6H_2O$ reported in this article does not seem to be influenced by the magnon-phonon interaction even though $T \ll T_{AE}$($T_{AE} = 6.0$ °K). The specific heat of $NiCl_2 \cdot 6H_2O$ also does not seem at first glance to be affected by this interaction. However, the (specific heat)/T^3 data shown in Fig. 2 of Ref. 26 seems to be leveling off, except for one datum point, rather than going to zero. The data points were fit to Eisele and Keffer's theory using a $T_{AE} = 4.0$ °K, while the T_{AE} predicted by antiferromagnetic resonance is about 6.5 ± 0.5 °K. If the aforementioned single datum point is ignored it seems that a good fit to the experimental data might be made by using a T_{AE} of about 6.5 °K, along with contributions to the specific heat from both Eisele and Keffer's theory and the magnon-phonon interaction. Of course, only experimental measurements of specific heat and T_1 at lower temperatures could settle this question. At any rate, the magnon-phonon interaction does not seem to be as important for $NiCl_2 \cdot 6H_2O$ as it seems to be for $CoCl_2 \cdot 6H_2O$ and $CuCl_2 \cdot 2H_2O$.

While the magnon-phonon interaction seems to be quite important for the specific heat in $CoCl_2 \cdot 6H_2O$, the T_1 measurements (down to 0.5 °K) do not display any indication of the direct relaxation process. This seems to be a contradictory bit of experimental evidence. In order to gain some insight into the problem, the ratio of the magnon-phonon process to the regular process will be taken. For the specific heat we have, according to Kimura[37]

$$C_{m\text{-}p}/C_{mag} \cong f(0, x_n)/f(x_0, x_m) , \tag{35}$$

where $f(0, x_n) \cong 0$ for $T > T_{AE}$, and goes to a maximum of about 25 as $T \to 0$; and $f(x_0, x_m) \to 0$ as $T \to 0$. For T_1 we have

$$\frac{\text{direct relaxation } (1/T_1)}{\text{two-magnon relaxation } (1/T_1)} \propto \frac{G^2 J^4}{T^2} . \tag{36}$$

G is the size of the magnon-phonon interaction and all terms that would be about the same for both $CoCl_2 \cdot 6H_2O$ and $CuCl_2 \cdot 2H_2O$ have been ignored. The expressions for relaxation due to direct processes and for the two-magnon processes were

taken from Refs. 4 and 5, respectively. It is seen from Eq. (36) that the importance of direct relaxation depends a great deal on the size of the exchange integral. If one assumes that G is about the same size in $CoCl_2 \cdot 6H_2O$ and $CuCl_2 \cdot 2H_2O$, then the direct relaxation process in $CoCl_2 \cdot 6H_2O$ would not be important until $T \lesssim 0.1\,^\circ K$ [assuming $J_{Co}/J_{Cu} = T_N(Co)/T_N(Cu) \simeq 2$], since only at $0.9\,^\circ K$ did this process become important in $CuCl_2 \cdot 2H_2O$. Thus, the assumption that the magnon-phonon interaction is physically important does not meet with any inconsistencies in the experimental data from specific-heat and T_1 measurements for these three crystals.

We conclude from the above discussion that the reported T^{-7} temperature dependence of T_1 and Pincus and Winter's[4] theory was merely fortuitous. Still, the magnon-phonon interaction may play a very important role for specific heat and T_1 measurements in the temperature range $T < T_{AE}$. An independent experimental value for G would be of value in determining this importance.

The increased line broadening found when $|\phi_{min} - \phi|$ was increased was explained by an inhomogeneous demagnetizing field set up by the component of the electron dipole field perpendicular to H_0.

The discontinuity in T_2 as a function of temperature for $NiCl_2 \cdot 6H_2O$ at $T = 2.1\,^\circ K$ was not explained.

A partial explanation was given for the enhancement of the rf signal when $\vec{H}_0 \| c$ axis in $CoCl_2 \cdot 6H_2O$.

ACKNOWLEDGMENTS

We wish to thank Professor F. Keffer and Professor S. Friedberg for many helpful discussions, and Professor S. Friedberg for giving us our "impure" crystal of $Ni_2Cl_2 \cdot 6H_2O$.

APPENDIX A: INTERACTION HAMILTONIAN FOR TWO- AND THREE-MAGNON SCATTERING PROCESSES AND THE THREE-MAGNON THERMAL-RELAXATION PROBABILITY

The approach to calculating the interaction Hamiltonian given in this Appendix is not original in detail and the two-magnon part is equivalent to Moriya's[2] method, but it is felt that the method used displays the interaction Hamiltonian in a fashion that clearly delineates which terms are responsible for the different relaxation processes. It also is necessary for calculating the orientation dependence of the dipole-dipole interaction coefficient $|h^{\pm}_{l,m}|^2$ carried out in Appendix B. We also show here what approximations were made in calculating $1/T_1^{(3)}$.

Using standard techniques,[40] the fluctuating part of the interaction Hamiltonian, denoted by $\mathcal{H}'$, and defined by Eq. (9), can be rewritten in terms of the spherical coordinates which are defined in Fig. 5.

Breaking up $\mathcal{H}'$ into $\mathcal{H}'_u$ for the "up" sublattice and $\mathcal{H}'_d$ for the "down" sublattice so that $\mathcal{H}' = \mathcal{H}'_u + \mathcal{H}'_d$, we find

$$\begin{aligned}\mathcal{H}'_u = \sum_l (g\mu_B \gamma_N \hbar / r_l^3) \{ & \delta S_z I_z (1 - 3\cos^2\theta_{IS}) \\ & - \tfrac{1}{4}[\delta S^+ I^- + \delta S^- I^+](1 - 3\cos^2\theta_{IS}) \\ & - \tfrac{3}{2}[\delta S^+ I_z + \delta S_z I^+] \sin\theta_{IS} \cos\theta_{IS} e^{-i\phi_{IS}} \\ & - \tfrac{3}{2}[\delta S^- I_z + \delta S_z I^-] \sin\theta_{IS} \cos\theta_{IS} e^{i\phi_{IS}} \\ & - \tfrac{3}{4} \delta S^+ I^+ \sin^2\theta_{IS} e^{-2i\phi_{IS}} \\ & - \tfrac{3}{4} \delta S^- I^- \sin^2\theta_{IS} e^{2i\phi_{IS}} \} \end{aligned} \quad (37)$$

and similarly for $\mathcal{H}'_d$. Since only the terms which contain δS_z contribute to Raman scattering (see Sec. III B), the terms from $\mathcal{H}'_u$ in which we are interested are

$$\begin{aligned}\mathcal{H}'_{u1} = \sum_l (g\mu_B \gamma_N \hbar / r_l^3) \delta S_z [& I_z (1 - 3\cos^2\theta_{IS}) \\ & - \tfrac{3}{2} \sin\theta_{IS} \cos\theta_{IS} (I^+ e^{-i\phi_{IS}} + I^- e^{i\phi_{IS}})] . \end{aligned} \quad (38)$$

The axis of quantization of the proton spins is different from that of the electron spins and the components of $\vec{I}$ must now be transformed to the primed coordinate system shown in Fig. 6. The axis z' is chosen to lie along $\vec{H}_{eff}$:

$$\begin{aligned} I^{\pm} &= \tfrac{1}{2}(I'^+ + I'^-)\cos\theta + I'_z \sin\theta \pm \tfrac{1}{2}(I'^+ - I'^-) , \\ I_z &= I'_z \cos\theta - \tfrac{1}{2}(I'^+ + I'^-)\sin\theta , \end{aligned} \quad (39)$$

where $I^{\pm} = I_x \pm iI_y$. The terms in $\mathcal{H}'_{u1}$ that cause nuclear-spin-lattice relaxation are $\delta S_z I'^+$ and $\delta S_z I'^-$, so that the other terms in $\mathcal{H}'_{u1}$ can be dropped. Denoting the surviving collected terms by $\mathcal{H}'_{u2}$ yields

$$\begin{aligned}\mathcal{H}'_{u2} = g\mu_B \gamma_N \hbar [& I'^+ \textstyle\sum_l h_l^+(\theta, \theta_{IS}, \phi_{IS}) \delta S_{lz} / r_l^3 \\ & + I'^- \textstyle\sum_l h_l^-(\theta, \theta_{IS}, \phi_{IS}) \delta S_{lz} / r_l^3] , \end{aligned} \quad (40)$$

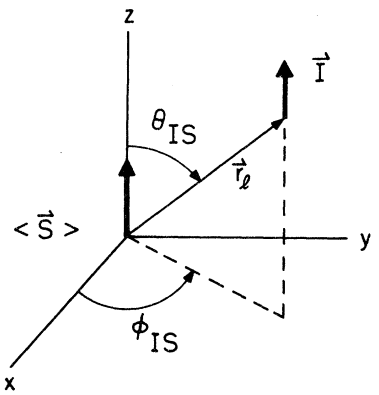

FIG. 5. Spherical coordinates used for the dipole-dipole interaction Hamiltonian.

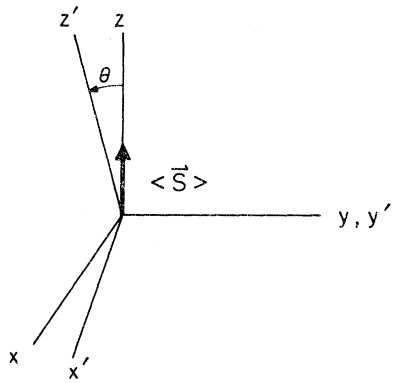

FIG. 6. Electron spins are quantized along the z axis and nuclear spins along the z' axis. The primed coordinate system has been rotated through the angle θ about the y axis. There is no loss of generality in having the y and y' axes coincident.

where

$$h_l^{\pm}(\theta, \theta_{IS}, \phi_{IS}) = -\tfrac{1}{2}[\sin\theta(1-3\cos^2\theta_{IS}) + 3(\cos\phi_{IS}\cos\theta \mp i\sin\phi_{IS})\sin\theta_{IS}\cos\theta_{IS}]\,. \tag{41}$$

By the same technique, $\mathcal{H}_d'$ transforms into $\mathcal{H}_{d2}'$ having the same form as $\mathcal{H}_{u2}'$ with l replaced by m.

We now introduce the magnon creation and destruction operators,

$$\begin{aligned}
&\delta S_l^+ = (2S)^{1/2} f_l\, a_l^-\,,\\
&\delta S_l^- = (2S)^{1/2} a_l^+ f_l\,,\\
&\delta S_{lz} = a_l^+ a_l^-\,,\\
&f_l = \left(1 - \frac{a_l^+ a_l^-}{2S}\right)^{1/2} \simeq 1 - \frac{a_l^+ a_l^-}{4S}\,,\\
&\delta S_m^+ = (2S)^{1/2} b_m^+ f_m\,,\\
&\delta S_m^- = (2S)^{1/2} f_m b_m^-\,,\\
&\delta S_{mz} = -b_m^+ b_m^-\,,\\
&f_m = \left(1 - \frac{b_m^+ b_m^-}{2S}\right)^{1/2} \cong 1 - \frac{b_m^+ b_m^-}{4S}\,;
\end{aligned} \tag{42}$$

f_l and f_m are expanded above in a binomial series and only the lowest-order terms are kept. Substituting Eq. (42) into Eq. (40) yields

$$\mathcal{H}_2' = I'^{+}\left(\sum_l C_{lz}^+ a_l^+ a_l^- - \sum_m C_{mz}^+ b_m^+ b_m^-\right) + I'^{-}\left(\sum_l C_{lz}^- a_l^+ a_l^- - \sum_m C_{mz}^- b_m^+ b_m^-\right), \tag{43}$$

where

$$C_{lz}^{\pm} = (g\mu_B \gamma_N \hbar) h_l^{\pm}(\theta, \theta_{IS}, \phi_{IS})/r_l^3\,, \tag{44}$$

with $C_{mz}^{\pm}$ having the same form with l replaced by m.

The δS^+ and δS^- operators contain three-magnon operators, and can thus produce nuclear-spin transitions involving three magnons. Picking out the terms in $\mathcal{H}'$ that contain a δS^+ or a δS^-, transforming these to the primed reference frame for the nuclear spins and keeping I'^{+} and I'^{-} terms yields

$$\mathcal{H}_3'' = I'^{+}\left[\sum_l (B_l^{++}\delta S_l^+ + B_l^{+-}\delta S_l^-) + \sum_m (B_m^{++}\delta S_m^+ + B_m^{+-}\delta S_m^-)\right] + I'^{-}\left[\sum_l (B_l^{-+}\delta S_l^+ + B_l^{--}\delta S_l^-) + \sum_m (B_m^{-+}\delta S_m^+ + B_m^{--}\delta S_m^-)\right], \tag{45}$$

where

$$B_l^{\pm\pm} = \frac{g\mu_B \gamma_N \hbar}{r_l^3}\, v_l^{\pm\pm}(\theta, \theta_{IS}, \Phi_{IS})\,, \tag{46a}$$

$$v_l^{+\pm}(\theta, \theta_{IS}, \phi_{IS}) = \pm\tfrac{1}{8}(1-3\cos^2\theta_{IS}) \mp \tfrac{3}{8}\sin^2\theta_{IS} e^{\mp 2i\Phi_{IS}} + (\cos\theta)\left[-\tfrac{1}{8}(1-3\cos^2\theta_{IS}) - \tfrac{3}{8}\sin^2\theta_{IS}\, e^{\mp 2i\Phi_{IS}}\right] + (\sin\theta)\left(\tfrac{3}{4}\sin\theta_{IS}\cos\theta_{IS}\, e^{\mp i\Phi_{IS}}\right), \tag{46b}$$

$$v_l^{-\pm}(\theta, \theta_{IS}, \Phi_{IS}) = \mp\tfrac{1}{8}(1-3\cos^2\theta_{IS}) \mp \tfrac{3}{8}\sin^2\theta_{IS}\, e^{\mp 2i\Phi_{IS}} + (\cos\theta)\left[-\tfrac{1}{8}(1-3\cos^2\theta_{IS}) - \tfrac{3}{8}\sin^2\theta_{IS}\, e^{\mp 2i\Phi_{IS}}\right] + (\sin\theta)\left[\tfrac{3}{4}\sin\theta_{IS}\cos\theta_{IS}\, e^{\mp i\Phi_{IS}}\right]; \tag{46c}$$

$B_m^{\pm\pm}$ may be found by replacing l by m in the above formulas. Substituting Eqs. (42) into Eq. (45) and dropping the one-magnon terms yields

$$\mathcal{H}_3' = -I'^{+}(2S)^{-1/2}\tfrac{1}{2}\left[\sum_l (B_l^{++} a_l^+ a_l^- a_l^- + B_l^{+-} a_l^+ a_l^+ a_l^-) + \sum_m (B_m^{++} a_m^+ a_m^- a_m^- + B_m^{+-} a_m^+ a_m^+ a_m^-)\right] - I'^{-}(2S)^{-1/2}\tfrac{1}{2}\left[\sum_l (B_l^{-+} a_l^+ a_l^- a_l^- + B_l^{--} a_l^+ a_l^+ a_l^-) + \sum_m (B_m^{-+} a_m^+ a_m^- a_m^- + B_m^{--} a_m^+ a_m^+ a_m^-)\right], \tag{47}$$

which is the interaction that causes three-magnon relaxation.

The usual transformations,[41]

$$a_k^+ = l_{1k} a_k^+ + l_{2k}\beta_k^-\,; \quad a_k^- = l_{1k}^* \alpha_k^- + l_{2k}^* \beta_k^+\,,$$

$$b_k^+ = l_{2k}\alpha_k^- + l_{1k}\beta_k^+\,; \quad b_k^- = l_{2k}^* \alpha_k^+ + l_{1k}^* \beta_k^-\,,$$

TABLE VII. Atom position parameters (Ref. 34) (fractions of unit cell length) in $CuCl_2 \cdot 2H_2O$. It is orthorhombic with lattice parameters $a = 7.38$ Å, $b = 8.04$ Å, and $c = 3.72$ Å. y is along the b axis and z is along the a axis.

Atom	x	y	z
Cu	0	0	0
O	0	0.2390	0
H	0.0822	0.3065	0.1295

TABLE VIII. Distances to four nearest Cu^{++} ions from a hydrogen atom in $CuCl_2 \cdot 2H_2O$. In Fig. 1, Ref. 34 this is the left hydrogen atom of the H_2O molecule located at the coordinates $(a, b) = (0.5, 0.8)$. Cu1 is located at (0.5, 0.5), Cu2 at (0,1.0), Cu3 at (1.0, 1.0), and Cu4 is located directly above Cu1 along the c axis.

	r	$1/r^3$	$1/r^6$
Cu1	2.58 Å	5.82×10^{-2} Å^{-3}	3.39×10^{-3} Å^{-6}
Cu2	4.59 Å	1.03×10^{-2} Å^{-3}	0.106×10^{-3} Å^{-6}
Cu3	3.48 Å	2.37×10^{-2} Å^{-3}	0.563×10^{-3} Å^{-6}
Cu4	4.41 Å	1.17×10^{-2} Å^{-3}	0.137×10^{-3} Å^{-6}

which diagonalizes the electron Hamiltonian, are applied to $\mathcal{H}_3'$ and the terms which contain all annihilation or all creation operators are left out, because energy cannot be conserved for these interactions.

The thermal transition probability is

$$W^{(3)}_{-1/2,1/2} = \frac{2\pi}{\hbar} \sum_{\nu,\nu'=1}^{2} \times \{ \sum_{k_1,k_2,k_3} [\langle | \langle n_{\nu k_1}+1, n_{\nu k_2}+1, n_{\nu k_3}-1; \times 1/2 | \mathcal{H}_3' | n_{\nu k_1}, n_{\nu k_2}, n_{\nu k_3}; -1/2 \rangle |^2 \rangle_{av} \times \delta(\hbar\omega_1+\hbar\omega_2-\hbar\omega_3)$$

$$+ \langle | \langle n_{\nu k_1}+1, n_{\nu k_2}-1, n_{\nu k_3}-1; 1/2 | \mathcal{H}_3' | n_{\nu k_1}, n_{\nu k_2}, n_{\nu k_3}; -1/2 \rangle |^2 \rangle_{av} \times \delta(\hbar\omega_1-\hbar\omega_2-\hbar\omega_3)] \} , \quad (48)$$

where the first term is the splitting process and the second term is the confluence process. In the sums in Eq. (48), care must be taken so as not to count the final states twice where interchange of 1 and 2 in the splitting process does not lead to a different final state or to count the initial states twice where interchange of 2 and 3 in the confluence process does not lead to a different initial state. This counting of states and subsequent calculation is shown in detail in Ref. 13.

Making the approximation

$$A_k/\hbar\omega \pm 1 \cong A_k/\hbar\omega , \quad (49)$$

replacing the sums by integrals, and integrating once to get rid of the δ function, we obtain

$$W^{(3)}_{-1/2,1/2} = \frac{9}{8}\pi(27)\,\frac{(g\mu_B\gamma_N)^2}{\theta_m^6}\,\frac{\hbar}{k_B} \times \left(\sum_l \frac{|h_l^{\pm}|^2}{r_l^6} + \sum_m \frac{|h_m^{\pm}|^2}{r_m^6} \right) \left(\frac{A_k}{\theta_m k_B} \right)^3 T^5 I_3(T_{AE}/T) , \quad (50)$$

where

$$I_3\left(\frac{T_{AE}}{T}\right) = \int_{x_{AE}}^{x_m}\int_{x_{AE}}^{x_m} \frac{(x_1^2-x_{AE}^2)^{1/2}(x_2^2-x_{AE}^2)^{1/2}[(x_1+x_2)^2-x_{AE}^2]^{1/2} e^{x_1+x_2}\,dx_1\,dx_2}{(e^{x_1+x_2}-1)(e^{x_2}-1)(e^{x_1}-1)} , \quad (51)$$

and it has been assumed that (order-of-magnitude estimate)

$$\sum_l (|B_l^{+\pm}|^2 + |B_l^{-\pm}|^2) + \sum_m (|B_m^{+\pm}|^2 + |B_m^{-\pm}|^2) \cong 2(\sum_l |C_{l\varepsilon}^{\pm}|^2 + \sum_m |C_{m\varepsilon}^{\pm}|^2) . \quad (52)$$

APPENDIX B: ESTIMATE OF THE SIZE AND THE TEMPERATURE DEPENDENCE OF THE DIPOLE-DIPOLE INTERACTION COEFFICIENT $|h_l^{\pm}|^2$

The dipole-dipole interaction coefficient $|h_l^{\pm}|^2$ depends on the angles θ, θ_{IS}, and ϕ_{IS} (see Figs. 5 and 6). In order to obtain a realistic value for this coefficient and its temperature dependence, we attempt here to approximate these angles and evaluate $|h_l^{\pm}|^2$, where $h_l^{\pm}$ is defined in Eq. (41).

This calculation will be carried out for $CuCl_2 \cdot 2H_2O$, because it has the simplest crystal structure of the three crystals investigated, orthorhombic as opposed to monoclinic, (because it has only two waters per unit cell instead of six as for the other two crystals), and because the literature pertaining to the theoretical and experimental investigations of it are the most extensive and thorough.

The proton positions in $CuCl_2 \cdot 2H_2O$ were found

TABLE IX. Values of $|\vec{H}_d|$, $\cos\theta$, and $|h_1^{\pm}|^2$ for several temperatures for $CuCl_2 \cdot 2H_2O$.

T(°K)	1.2	1.5	2.0	2.5	3.0	3.5	4.0
$\lvert\vec{H}_d\rvert$ (G)	760	755	745	722	682	615	471
$\cos\theta$	−0.674	−0.677	−0.681	−0.692	−0.709	−0.737	−0.833
$\lvert h_1^{\pm}\rvert^2$	0.237	0.236	0.2356	0.233	0.229	0.222	0.177

TABLE X. Values of T_{AE_1} and T_{AE_2} for several temperatures for $CuCl_2 \cdot 2H_2O$.

T(°K)	0.8	1.0	1.2	1.5	2.0	2.5	3.0	3.5	4.0
T_{AE_1}(°K)	0.975	0.975	0.975	0.963	0.939	0.887	0.801	0.693	0.468
T_{AE_2}(°K)	1.76	1.76	1.76	1.74	1.70	1.61	1.45	1.25	0.848

from neutron-diffraction experiments and are shown in Fig. 1 of Ref. 34. Useful atom position parameters are listed in Table VII; and distances to the four nearest Cu^{++} ions from a hydrogen atom are listed in Table VIII.

It is obvious from Table VIII that one need not go any further than the closest Cu^{++} ion in order to get a good approximation of

$$\sum_l \frac{|h_l^{\pm}|^2}{r_l^6} + \sum_m \frac{|h_m^{\pm}|^2}{r_m^6} \quad . \tag{53}$$

If we assume that Cu1 is on the "up" sublattice, then

$$\sum_l \frac{|h_l^{\pm}|^2}{r_l^6} + \sum_m \frac{|h_m^{\pm}|^2}{r_m^6} \simeq \frac{|h_1^{\pm}|^2}{r_1^6} = 3.39 \times 10^{45} |h_1|^2 \ \mathrm{cm}^{-6} , \tag{54}$$

where

$$|h_1^{\pm}|^2 = \tfrac{1}{4} |\sin\theta(1 - 3\cos^2\theta_{IS}) + 3\cos\phi_{IS}\cos\theta\sin\theta_{IS}\cos\theta_{IS} \mp i\, 3\sin\phi_{IS}\sin\theta_{IS}\cos\theta_{IS}|^2 , \tag{55}$$

and

$$\cos\theta_{IS} = 0.235; \quad \sin\theta_{IS} = 0.973 , \qquad \sin\phi_{IS} = 0.98; \quad \cos\theta_{IS} = -0.192 , \tag{56}$$

as defined by Fig. 5. It remains now to calculate θ, as defined by Fig. 6, in order to evaluate $|h_1^{\pm}|^2$.

This can be determined from the resonance diagrams given in Fig. 7, Ref. 16. By definition,

$$\cos\theta = \hat{z} \cdot \vec{H}_{eff} / |\vec{H}_{eff}| , \tag{57}$$

where the z axis is the axis of quantization for the electron spin system and

$$\vec{H}_{eff} = \vec{H}_0 + \vec{H}_d , \tag{58}$$

where $\vec{H}_d$ is the dipole field due to the electrons. Thus, we find

$$\cos\theta = \frac{1}{|\vec{H}_{eff}|} [H_0 + \cos\theta_d |\vec{H}_d|] , \tag{59}$$

where $\cos\theta_d$ is the angle between the z axis and $\vec{H}_d$.

When $H_0 = 0$ we have

$$2\pi f_0 = \gamma_N |\vec{H}_d| , \tag{60}$$

where f_0 is the nuclear resonance frequency and γ_N is the proton gyromagnetic ratio. From studies[39,42] of the proton resonance in $CuCl_2 \cdot 2H_2O$ for $H_0 = 0$ and for low temperatures such that $\langle S_z \rangle \cong \frac{1}{2}$ it is found that

$$f_0 = 3.24 \ \mathrm{MHz} \tag{61}$$

and thus

$$|\vec{H}_d|_{T\sim 0} = 760 \ \mathrm{G} . \tag{62}$$

Through the use of the resonance diagram in Fig. 7, Ref. 16, $\cos\theta_d$ can be determined. For $H_0 \neq 0$ the nuclear resonance field is given by

$$(\omega/\gamma_N)^2 = H_0^2 + 2H_0 |\vec{H}_d| \cos\phi + |\vec{H}_d|^2 , \tag{63}$$

where ϕ is the angle between $\vec{H}_0$ and $\vec{H}_d$. If H_0 is along the z axis (a axis in $CuCl_2 \cdot 2H_2O$) then $\phi = \theta_d$. For $\vec{H}_0$ along the z axis, the resonant frequency is $f = 9.6$ MHz, where f has been corrected for $\Delta\nu_p$, the shift in the resonant frequency due to the perpendicular component of the local field (see Ref. 16). Thus we have

$$\cos\theta_d = -0.61 . \tag{64}$$

If we now assume that $\vec{H}_0$ is 22° from the $-z$ axis in the y, z (a, b) plane and $|\vec{H}_0| = 1705$ G, then at $T = 1.19$ °K, $f \cong 4.8$ MHz, we have

$$\cos\theta = -0.99 \tag{65}$$

and finally

$$|h_1^{\pm}|^2 \cong 0.13 . \tag{66}$$

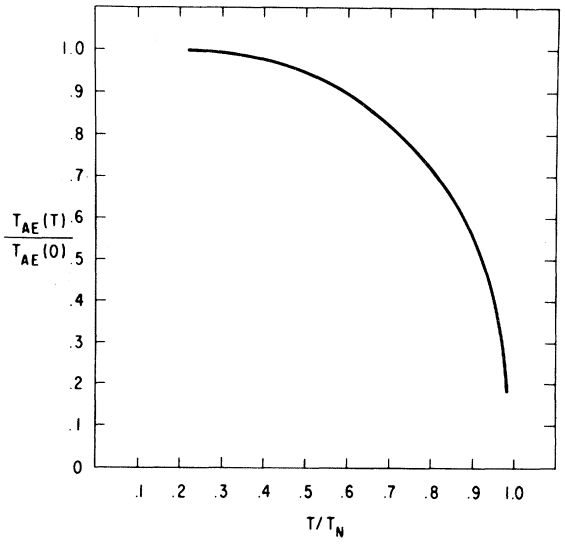

FIG. 7. T_{AE_1} as a function of T for $CuCl_2 \cdot 2H_2O$.

Combining this with the results of Eq. (54) leads to

$$\sum_l \frac{|h_l^{\pm}|^2}{r_l^6} + \sum_m \frac{|h_m^{\pm}|^2}{r_m^6} \cong 0.4 \times 10^{45}\ \mathrm{cm}^{-6}\ . \qquad (67)$$

$|h_l^{\pm}|^2$ is temperature dependent because the angle θ is a function of temperature. This follows from the dependence in Eq. (9) of $\vec{H}_{eff}$ on $\langle S_l \rangle$ which is temperature dependent. The data in Fig. 4 were taken with a constant frequency $f = 6.74$ MHz and with an external field $\vec{H}_0$ directed 22° from the a axis. The magnitude of $\vec{H}_0$ was varied in order to stay on resonance as the temperature was lowered. Thus, if Eq. (59) is to be used in order to find $\cos\theta$ as a function of temperature, H_0 and $|\vec{H}_d|$ must first be found as a function of temperature ($\cos\theta_d$ is constant for all temperatures). It was experimentally shown by Poulis *et al.*[42] that the relation

$$|\vec{H}_d| = |\vec{H}_d|_{T\to 0}\,(1 - 1.27 \times 10^{-3}\ T^4) \qquad (68)$$

holds in the temperature range $1.2 < T < 3.5$ °K (for

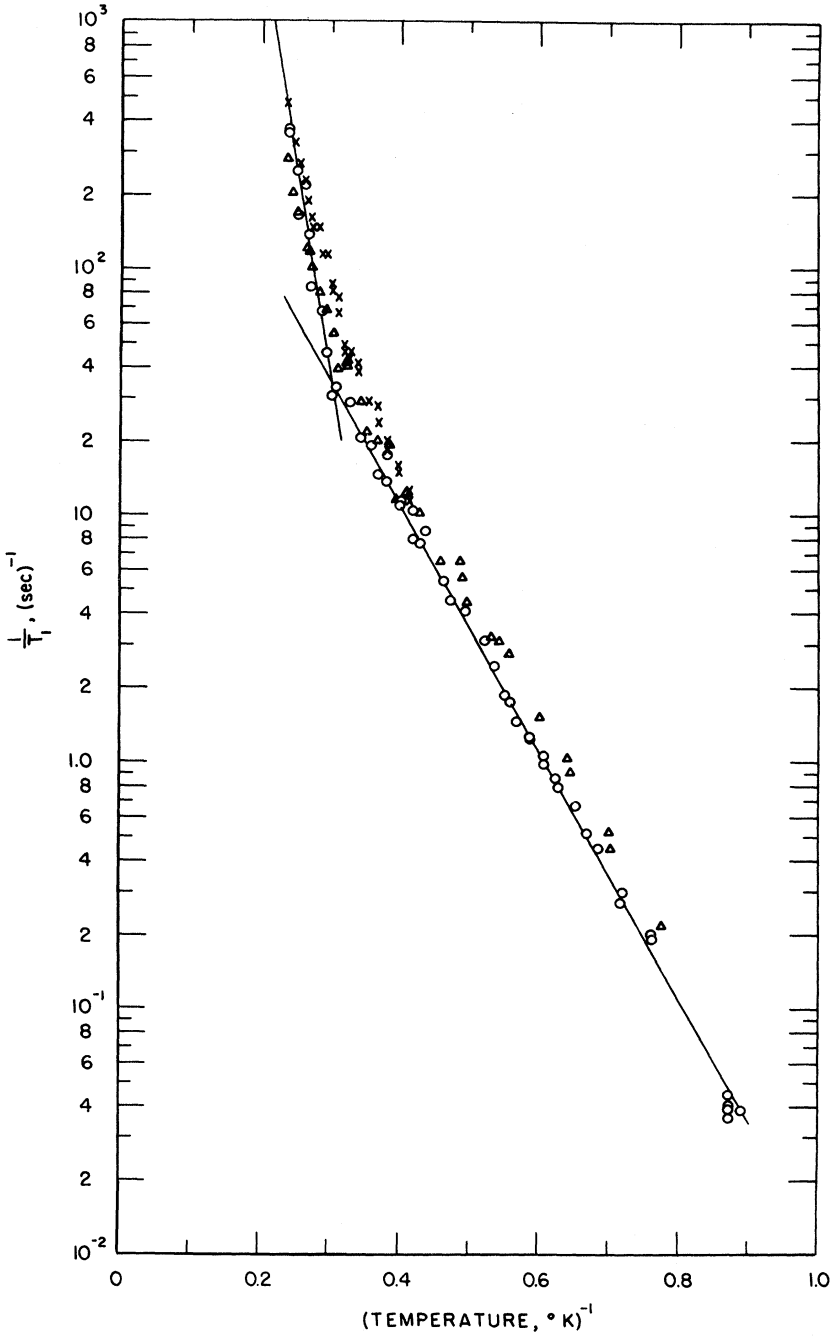

FIG. 8. $\mathrm{Log}_{10}(1/T_1)$ vs $1/T$ for protons $NiCl_2 \cdot 6H_2O$. The circles and ×'s are the experimental points found when five pulses and one pulse, respectively, were used to saturate the line in the pure sample (20 ppm). The triangles are the data from the 30 000-ppm sample.

$T \leq 1.2\,^{\circ}\mathrm{K}$ one can take $|\vec{H}_d| = |\vec{H}_d|_{T\to 0}$).

It only remains to determine H_0 as a function of temperature. This can be accomplished through the use of Eq. (63). The two variables in this equation, for this particular experiment, are H_0 and $|\vec{H}_d|$. If $\cos\phi$ was known, then H_0 would be a known function of $|\vec{H}_d|$. Figure 7, Ref. 16 can be used to find $\cos\phi$. At $T = 1.19\,^{\circ}\mathrm{K}$ and, for the maximum of a high-frequency line which lies between the a axis and the b axis: $f = 10.2$ MHz, $\vec{H}_0 = 1705$ G $(\cos 34.4^{\circ}\hat{z} + \sin 34.4^{\circ}\hat{y})$, $\vec{H}_d = 760$ G $(\hat{x}\sin\theta_d \times\cos\phi_d + \hat{y}\sin\theta_d \sin\phi_d + \cos\theta_d \hat{z})$ and thus:

$$\vec{H}_0 \cdot \vec{H}_d = (\sin\theta_d \sin\phi_d \sin 34.4^{\circ} + \cos\theta_d \cos 34.4^{\circ}) \times (760)(1705)\ \mathrm{G}^2$$

$$= [(0.79)\sin\phi_d (0.56) + (0.61)(0.83)] \times (762)(1705)\ \mathrm{G}^2$$

$$= \frac{1}{2}\left[\left(\frac{2\pi(10.2)\times 10^6}{2.68\times 10^4}\right)^2 - (1705)^2 - (760)^2\right] \mathrm{G}^2 , \tag{69}$$

where the last line comes from Eq. (63), and finally

$$\sin\phi_d = 0.8 . \tag{70}$$

In the relaxation experiment, $\vec{H}_0 = H_0(\sin 22^{\circ}\hat{y} - \cos 22^{\circ}\hat{z})$ and

$$\cos\phi = (0.79)(0.8)(0.37) - (0.61)(0.927) = -0.33 . \tag{71}$$

This gives us H_0 as a function of $|\vec{H}_d|$,

$$H_0^2 - 0.66|\vec{H}_d| H_0 + (|\vec{H}_d|^2 - 2.49\times 10^4) = 0 . \tag{72}$$

Solving this quadratic equation gives

$$H_0 = \tfrac{1}{2}[0.66|\vec{H}_d| + (9.96\times 10^6 - 3.56|\vec{H}_d|^2)^{1/2}] \tag{73}$$

and Eq. (59) becomes

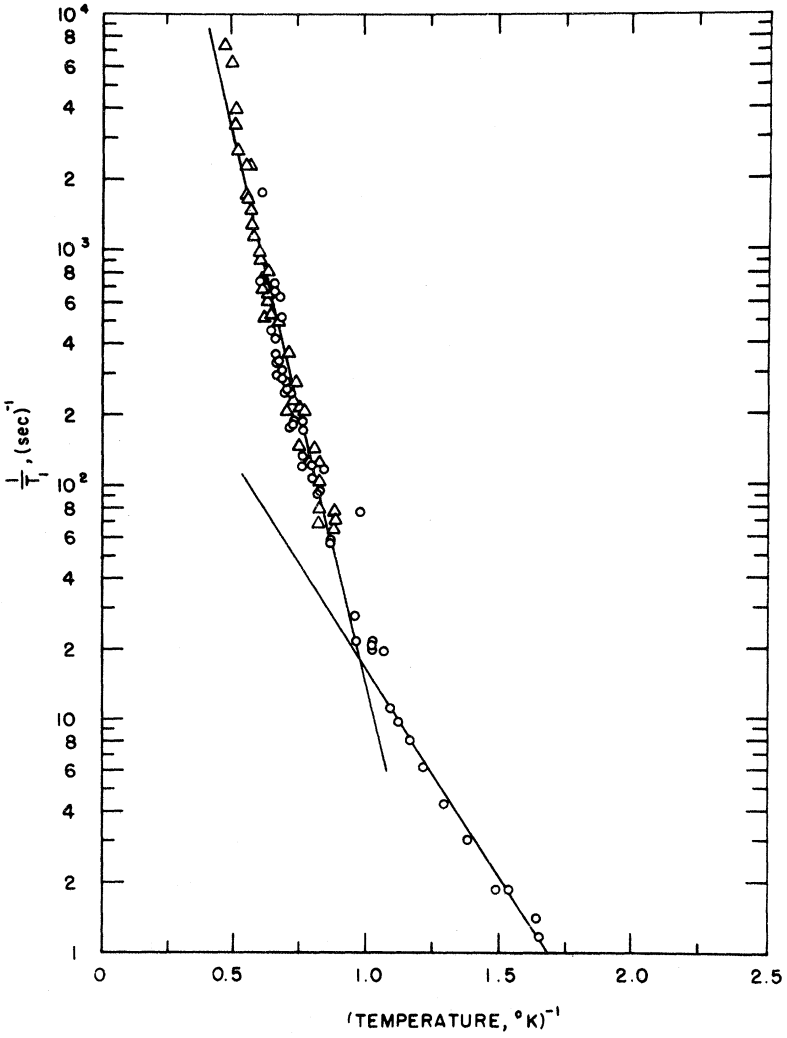

FIG. 9. $\mathrm{Log}_{10}(1/T_1)$ vs $1/T$ for $CoCl_2 \cdot 6H_2O$. The triangles and the circles are the data points for the proton and the ^{35}Cl resonance, respectively.

$$\cos\theta = \tfrac{1}{1579}\,[0.3\,|\vec{H}_d| - 0.46\,(9.96\times 10^6 - 3.56\,|\vec{H}_d|^2)^{1/2}]\,. \quad (74)$$

From Table IX it is seen that $|h_1^+|^2$ does depend on temperature but not very strongly. For $T = 4.0^\circ$K, $1/T_1^{(3)}$ should be multiplied by $\frac{3}{4}$ in order to correct for the temperature dependence of $|h_1^+|^2$. This is seen to be a small correction when compared to the overshoot caused by the small-$\vec{k}$ approximation.

APPENDIX C: T_{AE} AS A FUNCTION OF T

When an external magnetic field $\vec{H}_0$ is applied along the easy axis (a axis is $CuCl_2 \cdot 2H_2O$) and is increased, there occurs a value of H_0 for which the electron spins "flop" over perpendicular to the applied field. The field value necessary to do this is called the critical field H_c and varies considerably from crystal to crystal. This critical field is a good measure of T_{AE}, in fact (see Ref. 41, Chap. 40),

$$k_B\,T_{AE} \cong g\mu_B\,H_c\,(1-\chi_\parallel/\chi_\perp)^{1/2}\,. \quad (75)$$

Also, if we set

$$k_B\,T_{AE_1} \cong 2S(2z_1|J_1|K_1)^{1/2} \cong g\mu_B\,H_c\,(1-\chi_\parallel/\chi_\perp)^{1/2} \quad (76)$$

and use[43]

$$K_2 = 3.3\,K_1\,, \quad (77)$$

which means

$$T_{AE_2} \cong (3.3)^{1/2}\,T_{AE_1}\,, \quad (78)$$

we have T_{AE_1} and T_{AE_2} (assuming orthorhombic symmetry) as a function of T (since H_c and $\chi_\parallel$ are known functions of temperature). Poulis and

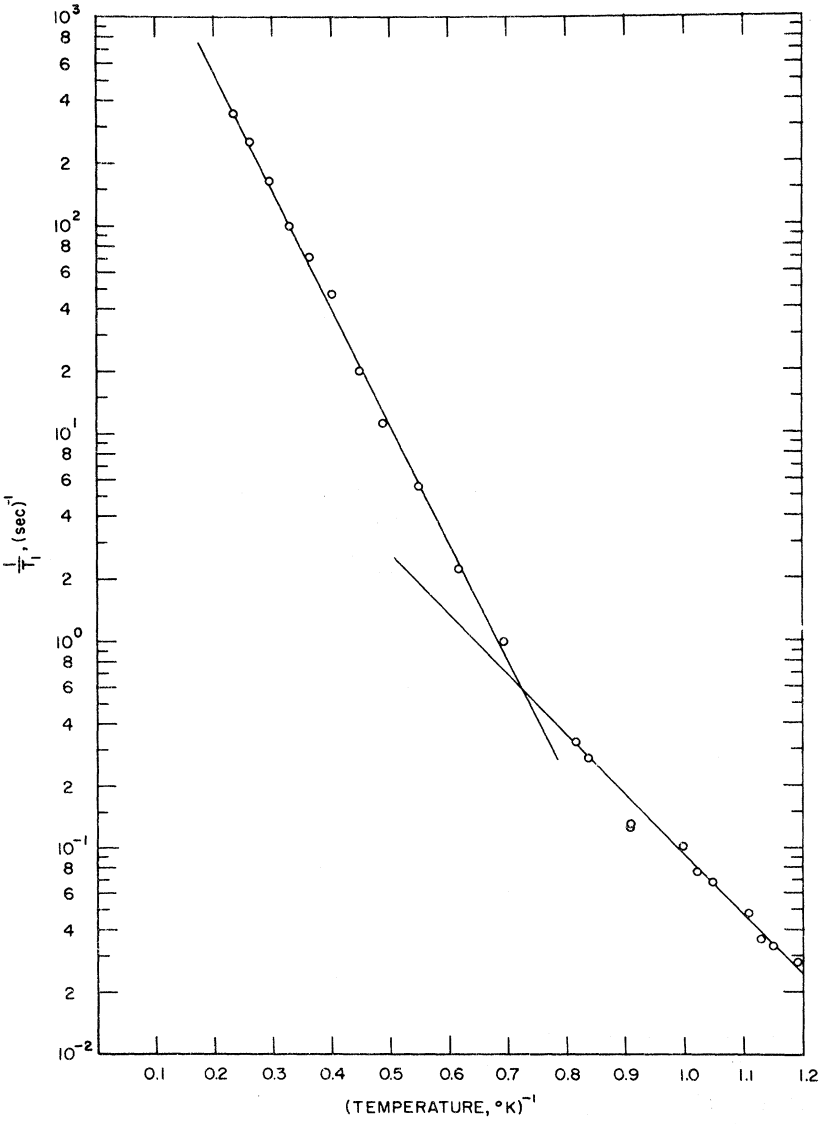

FIG. 10. $\mathrm{Log}_{10}(1/T_1)$ vs $1/T$ for $CuCl_2 \cdot 2H_2O$. The data are taken from Hardeman *et al.* (Ref. 1).

Hardeman[44] have found H_c as a function of temperature and $(1-\chi_{\parallel}/\chi_{\perp})$ has been plotted by Magamiya[43] as a function of temperature. The results for T_{AE_1} and T_{AE_2} are shown in Table X and Fig. 7. The temperature dependence of T_{AE_1} is found to be an important correction in Sec. IV, especially for $NiCl_2 \cdot 6H_2O$.

APPENDIX D: FIT OF T_1 DATA BY EXPONENTIAL FUNCTIONS

A plot of $\log_{10}(1/T_1)$ data against the reciprocal of the temperature (Figs. 8–10) shows that the data may be reasonably well fitted by the function

$$1/T_1 = C_1 e^{-\alpha_1/T} + C_2 e^{-\alpha_2/T}, \tag{79}$$

with different values of C_1, C_2, α_1, and α_2 for each of the crystals. For $NiCl_2 \cdot 6H_2O$ from Fig. 8,

$$\alpha_1 = 11.1\,^\circ\mathrm{K}, \quad \alpha_2^{(S)} = 40\,^\circ\mathrm{K}, \quad \alpha_2^{(1)} = 25\,^\circ\mathrm{K}; \tag{80}$$

for $CoCl_2 \cdot 6H_2O$ from Fig. 9,

$$\alpha_1 = 4\,^\circ\mathrm{K}, \quad \alpha_2 = 10\,^\circ\mathrm{K}; \tag{81}$$

and for $CuCl_2 \cdot 2H_2O$ we have, from Fig. 10,

$$\alpha_1 = 6.67\,^\circ\mathrm{K}, \quad \alpha_2 = 12.5\,^\circ\mathrm{K}. \tag{82}$$

α_1 is fit to the low-temperature values and α_2 to the high-temperature values. For $NiCl_2 \cdot 6H_2O$, $\alpha_2^{(S)}$ stands for the α_2 found when a series of pulses were used to saturate the line and $\alpha_2^{(1)}$ when just one pulse was used. (Note: The 30 000-ppm crystal has an α_1 which agrees with that of the other two $NiCl_2 \cdot 6H_2O$ crystals and an $\alpha_2 \cong \alpha_2^{(1)} = 25$.)

For $NiCl_2 \cdot 6H_2O$ and $CoCl_2 \cdot 6H_2O$, α_1 is about twice as large as their respective T_{AE}'s, but for $CuCl_2 \cdot 2H_2O$ it is about a factor of 6 larger. This inconsistency in α_1 makes this fit of the data less attractive than the two-magnon and three-magnon processes discussed in the body of the text. Also, there is no theory at present which predicts this double exponential behavior over the temperature range studied here.

---

†Partially based upon work presented by D. Whitson to the Department of Physics, University of Pittsburgh, in partial fulfillment of the requirement for a Ph.D. degree (1969).

*Work supported by the U. S. Air Force Office of Scientific Research, under Grant No. 196-1678.

‡NASA Predoctoral Fellow.

§Present address: Department of Physics, Indiana University of Pennsylvania, Indiana, Pa. 15701.

[1]G. E. G. Hardeman, N. J. Poulis, W. Van Der Lugt, and W. P. A. Hass, Physica 23, 907 (1957).

[2]Toru Moriya, Progr. Theoret. Phys. (Kyoto) 16, 23 (1956).

[3]J. Van Kranendonk and M. Bloom, Physica 22, 545 (1956).

[4]P. Pincus and J. Winter, Phys. Rev. Letters 7, 269 (1961).

[5]D. Beeman and P. Pincus, Phys. Rev. 166, 359 (1968).

[6]M. Abkowitz and I. J. Lowe, Phys. Rev. 142, 333 (1966).

[7]J. A. Cowen and C. E. Taylor, Phys. Letters 24A, 373 (1967).

[8]R. J. Mahler, A. C. Daniel, and P. T. Parrish, Phys. Rev. Letters 19, 85 (1967).

[9]I. J. Lowe and C. E. Tarr, J. Sci. Instr. 1, 604 (1968).

[10]I. J. Lowe and C. E. Tarr, J. Sci. Instr. 1, 320 (1968).

[11]P. Groth, *Chemische Krystallographie*, 1, *Teil* (Wilhelm Engelman Verlap, Leipzig, 1906), pp. 247 and 248.

[12]E. Sawatzky and M. Bloom, Can. J. Phys. 42, 657 (1964).

[13]D. W. Whitson, Ph.D. thesis (University of Pittsburgh, 1969) (unpublished).

[14]Johnson-Matthey Co.

[15]Mellon Institute, Pittsburgh, Pa.

[16]N. J. Poulis and G. E. G. Hardeman, Physica 18, 201 (1952).

[17]A. Brooks Harris, J. Phys. C 2, 463 (1969).

[18]J. Uhbink, J. A. Poulis, H. J. Gerritsen, and G. J. Gorter, Physica 18, 361 (1952).

[19]Kei Yosida, Progr. Theoret. Phys. (Kyoto) 7, 425 (1952).

[20]M. Date and M. Motokawa, J. Phys. Soc. Japan 22, 165 (1967).

[21]M. Date, J. Phys. Soc. Japan 16, 1337 (1961).

[22]J. Van den Handel, H. M. Gijsman, and N. J. Poulis, Physica 18, 862 (1952).

[23]R. Kleinberg, J. Appl. Phys. 38, 1453 (1967).

[24]A. Hamburger and S. A. Friedberg (unpublished).

[25]Z. M. El Saffer, J. Phys. Soc. Japan 21, 1844 (1966).

[26]R. H. Donaldson and D. T. Edmonds, Proc. Phys. Soc. (London) 85, 1209 (1965).

[27]Izuru Kimura and Norikiyo Urgy, J. Chem. Phys. 45, 4368 (1966).

[28]A. Nakumura, V. Minkiewicz, and A. M. Portis, J. Appl. Phys. 35, 842 (1964).

[29]N. Kaplan, R. Loudon, V. Jaccarino, H. J. Guggenheim, D. Beeman, and P. A. Pincus, Phys. Rev. Letters 17, 357 (1966).

[30]A. J. Heeger and D. T. Teany, J. Appl. Phys. 35, 846 (1964).

[31]R. J. Mahler and L. W. James, Bull. Am. Phys. Soc. 12, 1117 (1967).

[32]D. Harker, Z. Krist. 93, 136 (1936).

[33]G. Shirane, B. C. Frazer, and S. A. Friedberg, Phys. Letters 17, 95 (1965).

[34]S. W. Peterson and Henri A. Levy, J. Chem. Phys. 26, 220 (1957).

[35]A. C. Hewson, D. ter Haar, and M. E. Lines, Phys. Rev. 137, A1465 (1965).

[36]A. B. Harris (private communication).

[37]Izuru Kimura (private communication).

[38]J. A. Eisele and F. Keffer, Phys. Rev. 96, 929 (1954).

[39]H. Benolt and J. P. Renard, Phys. Letters 8, 32 (1964).

[40]C. P. Slichter, *Principles of Magnetic Resonance*

(Harper and Row, New York, 1963), p. 47.

[41]F. Keffer, *Handbuch der Physik*, edited by S. Flügge (Springer-Verlag, Berlin, 1966), Vol. 18.

[42]N. J. Poulis, G. E. G. Hardeman, W. van der Lugt, and W. P. A. Hass, Physica 24, 280 (1958).

[43]T. Nagamiya, Progr. Theoret. Phys. (Kyoto) 11, 309 (1954).

[44]N. J. Poulis and G. E. G. Hardeman, Physica 20, 7 (1954).